8-2016

Supervisory Control Optimization for a Series Hybrid Electric Vehicle with Consideration of Battery Thermal Management and Aging

Xueyu Zhang
Clemson University, xueyuz@clemson.edu

Supervisory Control Optimization for a Series Hybrid Electric Vehicle with Consideration of Battery Thermal Management and Aging

---

A Dissertation
Presented to
the Graduate School of
Clemson University

In Partial Fulfillment
of the Requirements for the Degree
Doctor of Philosophy
Automotive Engineering

---

by
Xueyu Zhang
August 2016

Accepted by:
Dr. Zoran Filipi, Committee Chair
Dr. Simona Onori
Dr. Pierluigi Pisu
Dr. Robert Prucka

ABSTRACT

This dissertation integrates battery thermal management and aging into the supervisory control optimization for a heavy-duty series hybrid electric vehicle (HEV). The framework for multi-objective optimization relies on novel implementation of Dynamic Programing algorithm and predictive models of critical phenomena. Electrochemistry based battery aging model is integrated into the framework to assess the battery aging rate by considering instantaneous lithium ion (Li^+) surface concentration rather than average concentration. This creates a large state-action space. Therefore, the computational effort required to solve a Deterministic or Stochastic Dynamic Programming becomes prohibitively intense, and a neuro-dynamic programming approach is proposed to remove the 'curse of dimensionality' in classical dynamic programming.

First, a unified simulation framework is developed for in-depth studies of series HEV system. The integration of a refrigerant system model enables prediction of energy use for cooling the battery pack. Side reaction, electrolyte decomposition, is considered as the main aging mechanism of $LiFePO_4$/Graphite battery, and an electrochemical model is integrated to predict side reaction rate and the resulting fading of capacity and power. An approximate analytical solution is used to solve the partial difference equations (PDEs) for Li^+ diffusion. Comparing with the finite difference method, it largely reduces the number of states with only a slight penalty on prediction accuracy. This improves

computational efficiency, and enables inclusion of the electrochemistry based aging model in the power management optimization framework.

Next, a stochastic dynamic programming (SDP) approach is applied to the optimization of supervisory control. Auxiliary cooling power is included in addition to vehicle propulsion. Two objectives, fuel economy and battery life, are optimized by weighted sum method. To reduce the computation load, a simplified battery aging model coupled with equivalent circuit model is used in SDP optimization; Li^+ diffusion dynamics are disregarded, and surface concentration is represented by the average concentration. This reduces the system state number to four with two control inputs. A real-time implementable strategy is generated and embedded into the supervisory controller. The result shows that SDP strategy can improve fuel economy and battery life simultaneously, comparing with Thermostatic SOC strategy. Further, the tradeoff between fuel consumption and active Li^+ loss is studied under different battery temperature.

Finally, the accuracy of battery aging model for optimization is improved by adding Li^+ diffusion dynamics. This increases the number of states and brings challenges to classical dynamic programming algorithms. Hence, a neuro-dynamic programming (NDP) approach is proposed for the problem with large state-action space. It combines the idea of functional approximation and temporal difference learning with dynamic programming; in that case the computation load increases linearly with the number of parameters in the approximate function, rather than exponentially with state space. The result shows the ability of NDP to solve complex control optimization problem reliably and efficiently. The battery-aging conscientious strategy generated by NDP optimization framework further improves battery life by 3.8% without penalty on fuel economy, compared to SDP strategy. Improvements of battery life compared to the heuristic strategy are much larger, on the order of 65%. This leads to progressively larger fuel economy gains over time.

ACKNOWLEDGMENTS

First and foremost, I would like to express my deepest gratitude to my advisor, Prof. Zoran Filipi. He provided me with a great opportunity to work on this interesting and challenging research topic, and continued to support me throughout my Ph.D studies. His patient guidance, trust, and encouragement helped me overcome all challenges in the past five years, and are deeply appreciated.

I am thankful to my committee members, Professors Simona Onori, Pierluigi Pisu, and Robert Prucka for their advice and comments on my dissertation. And I thank Prof. Andrej Ivanco for sharing his knowledge and patiently answering all my questions. I've enjoyed the collaborative work with Dr. Xinran Tao and Prof. John Wagner, and I am grateful to them for contributing the cooling model and battery thermal management.

I wish to express my gratitude to the Department of Automotive Engineering for providing an excellent and stimulating study environment. I thank all staff for their kind help and access to state-of-the-art faculties.

I would like to acknowledge the financial support from the Automotive Research Center (ARC) led by the University of Michigan, a U.S. Army center of excellence in modeling and simulation of ground vehicles funded by US Army TARDEC, Warren.

TABLE OF CONTENTS

Table of Contents (Continued)

Page

LIST OF TABLES

LIST OF FIGURES

List of Figures (Continued)

Figure Page

List of Figures (Continued)

CHAPTER ONE

INTRODUCTION

1.1 Research Motivation and Challenges

Energy security and reduced green-house gas emissions have spurred intense research efforts focusing on hybrid electric propulsion systems for cars and trucks. When it comes to military trucks, the research drivers are somewhat different, but equally strong. Development of hybrid electric propulsion for military trucks is expected to reduce the dependency on foreign oil, to increase the sustainability, to increase force protection, and to reduce the logistics tail, i.e. the number of fuel convoys. In addition, the military needs a significant level of electric power onboard to meet the requirement of warfighter's reside and weapon operation, and requirement for silent watch and high mobility (Khalil et al., 2009). Vehicle electrification has shown great potential for reducing fuel consumption and pollutant emissions. The main mechanisms for improving vehicle fuel efficiency are: (i) regeneration, due to the presence of a reversible secondary power source and energy storage, (ii) optimization of engine operation, (iii) engine down-sizing, and (iv) possibility for engine shut-downs. In particular, a series hybrid electric vehicle (S-HEV) offers ultimate freedom in controlling engine operation, and maximum regeneration capability, due to generous size of traction motors, and high mobility with independent wheel propulsion.

However, there are several challenges to applying the Series HEV concept to heavy off-road vehicles. Aggressive driving missions impose extraordinary power requirements and severe load cycles on electric components, such as batteries and electric motors, and both require cooling. In case of the battery pack, heat generates during battery usage, and the elevated battery internal temperature accelerates battery aging, and hence increases the cost for replacement. Further temperature increase will cause damage from thermal runaway. Requirement for battery safe operation and guaranteed usage lifetime in extreme ambient conditions mandates application of a refrigerant-based cooling. This leads to high auxiliary losses.

From commercial vehicles' perspective, the depletion of fuel resources and air pollution prevention forces the implementation of hybrid electric powertrain system. However, limited electric range and battery replacement cost are the main barrier to the widespread electrification of passenger cars. Previous studies has shown that battery operation temperature and load cycle have great impact on electric cars' range. Haaren et al. (Haaren et al., 2011) made a survey to assess the electric cars' range; as shown in Figure 1.1, in the highway in summer, the electric range is around only half of the ideal condition. This leads to more frequent recharging. Full recharging takes longer time than refueling, usually ranging from 30 minutes up to 48 hours. Battery life is another challenge. As shown in Figure 1.2 and 1.3, years of usage lead to the irreversible loss of battery capacity (Smith et al., 2015) and increase of internal resistance (Thomas et al., 2008). Elevated temperature will accelerate this fading phenomenon. To guarantee the performance at the end of battery life, the battery pack used in to be oversized. For example, the battery pack used in Chevy Volt is 16 kWh, and only 50% is used. The state of charge (SOC) is not allowed to fall below 40% or to increase above 90%. The oversizing was needed to meet the worst-case duty cycle and environments.

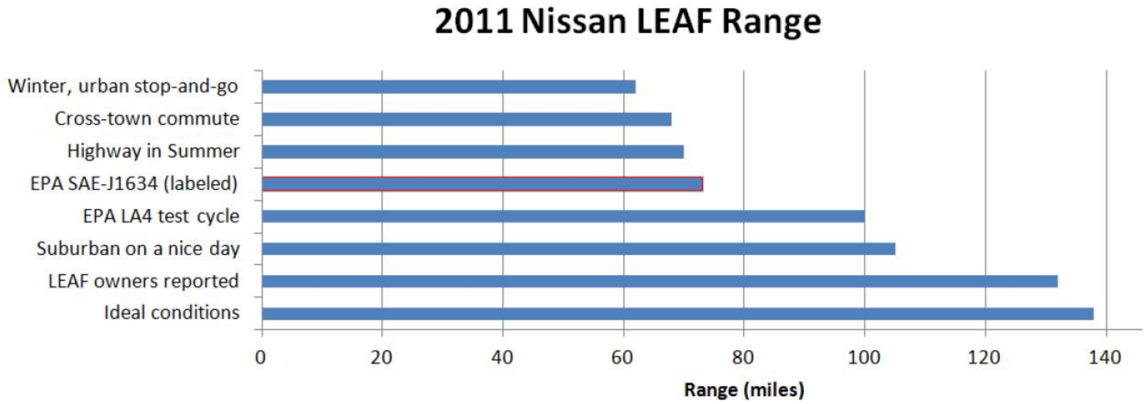

Figure 1.1: Range scenarios of the 2011 Nissan LEAF and the vehicle's EPA Fuel Economy sticker value (highlighted) (Haaren et al., 2011)

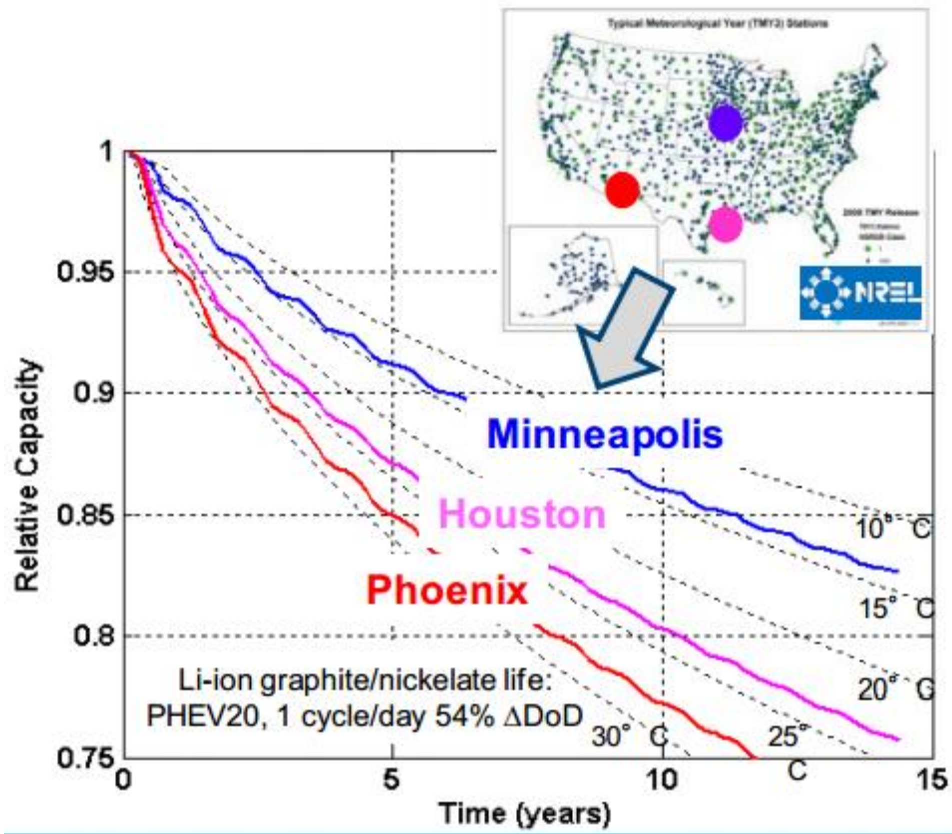

Figure 1.2: Relative capacity loss: Li-ion graphite/nickelate battery, 1cycle/day, 54% ΔDOD (Smith et al., 2015)

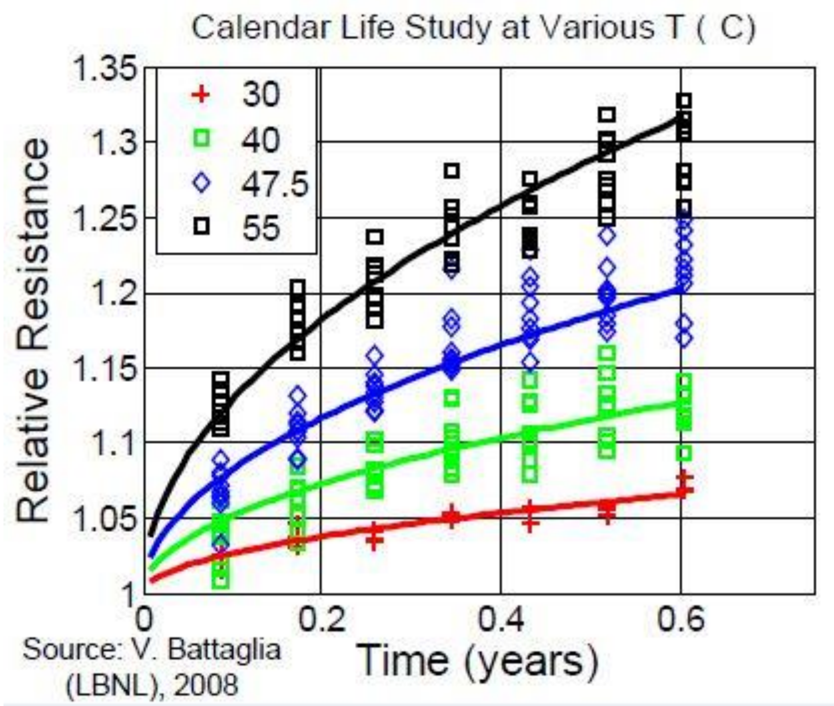

Figure 1.3: Relative Resistance increase (Thomas et al., 2008)

1.2 Objectives

The overarching goal of this dissertation is to develop a framework for multi-variable, multi-objective optimization of the hybrid-electric supervisory control. The impetus is driven by the need for fuel efficient and clean vehicles with endurance and resilience. The hybrid propulsion systems enable simultaneously improvements of efficiency, mobility, and flexibility in supporting electric devices on-board. However, the systems are complex; the design of supervisory control is critical for achieving simultaneous improvements of multiple vehicle attributes. Hence, advanced methodologies are required for systematic optimization of the supervisory control for a choice of relevant objectives.

In this study, we focus on the optimization of supervisory control with objectives of fuel economy and battery life. Battery thermal management and vehicle power management are integrated, and it takes the advantage of system flexibility to reduce the parasitic auxiliary losses. A computationally efficient optimization framework is designed capable of generating an optimal policy for multiple objectives. Critical elements required to build the framework are:

- A predictive simulation tool for in-depth analysis of powertrain system
- Optimal control algorithm suitable for multiple objectives, capable of handling large state-action space
- Able to generate real-time implementable strategy

1.3 Literature Review

1.3.1 Hybrid Powertrain Power Management

Vehicle electrification brings significant benefits for improving vehicle efficiency, but increases complexity, since vehicle can be driven by the engine, electric system, or their combination. Supervisory controller orchestrates operation of components in the powertrain system depending on driver's command and system states. It is critical for achieving the maximum benefits of any given hardware. This section reviews the supervisory control strategies that have been applied for the power management of HEVs.

A significant body of work on supervisory control strategies for hybrids has been published, and it can be grouped in several categories. The first category is heuristic-based strategy (Kim et al., 2007) (Jalil et al., 1997) (Salman et al., 2000) (Hofman et al.,2008). In case of the series HEVs, most commonly used heuristic strategy is Thermostatic SOC control. In this strategy, the power demand of power pack (engine coupled with generator) depends on the value of SOC, the goal is to sustain the SOC within reasonable range. Engine operating torque and rotation speed are controlled in a manner that ensures optimal efficiency of the engine and generator. It is robust and simple to implement, but the efficiency performance relies highly on engineer's experience and vehicle duty cycle. Johri et al. (Johri et al., 2009) has shown that the optimal system efficiency requires a more sophisticated strategy than a bang-bang controller.

To explore hybrids' full potential, optimization algorithms are proposed to solve HEV power management as an optimal control problem, with objective of maximizing the whole powertrain system efficiency instead of only focusing on engine/generator efficiency. The system transient function and objective function is defined as Eq. 1.1 and 1.2, respectively, with constrained state variables and control inputs.

$$x_{t+1} = f(x_t, u_t) \tag{1.1}$$

$$\min J = \int_{t_0}^{t_f} g(x_t, u_t, t)\,\mathrm{dt} \tag{1.2}$$

Subject to:

$$
\begin{aligned}
x_t &\in X \\
u_t &\in U
\end{aligned}
\tag{1.3}
$$

where x_t represents the state variables at time t, and u_t are control inputs. $g(x_t, u_t)$ is the instantaneous cost, which is a function of states and control inputs. The objective is to minimize the sum of instantaneous cost from t_0 to t_f. In case of HEV, the state x_t is usually defined as battery state of charge, and the instantaneous cost is defined as the fuel rate. The objective is to minimize the total fuel consumption over a period of driving mission.

Equivalent consumption minimization strategy (ECMS) was proposed to optimize the fuel consumption instantaneously (Musardo et al., 2005) (Serrao et al., 2009) (Onori et al., 2011) (Serrao et al., 2011) (Lescot et al., 2010) (Nüesch et al., 2014). The idea is to associate the use of the electrical energy buffer to a virtual increase or decrease of fuel consumption. The battery power consumption is converted into equivalent fuel consumption by an equivalence factor, and the objective is to minimize the sum of the real fuel consumption and the equivalent fuel consumption. With this strategy, the global minimization over time is simplified to optimize the instantaneous cost at every time step, and this assumption leads to sub-optimum. The equivalence factor is highly cycle dependent. ECMS was further developed (Musardo et al., 2005) (Gu et al., 2006) (Onori et al., 2011) for real-time implementation by adjusting the equivalence factor online using the driving cycle prediction or driving pattern recognition.

Pontryagin's Minimum Principle (PMP) has been proposed more recently (Rousseau et al., 2007) (Chasse et al., 2010) (Namwook et al., 2011) (Kim et al., 2012)

(Li et al., 2014) (Maamria et al., 2015). The optimal control solution is obtained by minimizing the Hamiltonian equation is defined as Eq. 1.4

$$H = g + \lambda(t) * \dot{x} \tag{1.4}$$

where λ(t) is time-relevant costate.

To simplify the computation process and make the PMP as a real-time control strategy, the costate is pre-calculated beforehand, and then the instantaneous Hamiltonian equation can be solved online (Namwook et al., 2011) (Li et al., 2014).

Model predictive control (MPC) was proposed by (Borhan et al., 2009) (Minh et al., 2012). In this algorithm, a linearized system model is used to predict the future responses of a system, and the prediction is used for calculating the optimal control input. The linearization calculation compromises the prediction accuracy for system response and computation load. In case of a complex system, the nonlinear MPC was proposed (Borhan et al., 2010) (Borhan et al., 2012). It requires high computation load; however, comparing with linear MPC, a noticeable improvement has been found by nonlinear MPC controller (Borhan et al., 2012).

One of the best known off-line optimization approaches is dynamic programming (DP) (Wu et al., 2002) (Neuman et al., 2009) (Lin et al., 2012) (Ebbesen et al., 2012). It is a powerful global optimization tool for solving complex problems. With the vehicle driving mission as a prior knowledge, the algorithm divides the whole problem into sub-problems and solves the cost-to-go function by backward iterations. DP strategy is cycle dependent, and hence cannot be implemented directly into real time control. It provides the benchmark for supervisory controller design. For real-time implementation, two methods have been proposed. The first method is to extract rules from the benchmark, and generate rule-base strategies. The second is to replace the known future with a probability of driver action and create a stochastic dynamic programming (SDP) framework (Lin et al., 2004) (Lars et al., 2007) (Moura et al., 2013). A stochastic driving cycle is modeled as Markov chain. SDP strategy is sub-optimal, but can be used for real-time application, as it is able to obtain time-invariant control strategy by solving an infinite-horizon optimization problem over the probability density function of future driving mission.

Fully integrated system with multiple objectives increases the number of states and control actions. Classical dynamic programming algorithm suffers from the curse of dimensionality (Powell et al., 2011); the computation load increases exponentially with the number of states, since the algorithm requires calculation of the cost-to-go function (value function) for every combination of discretized grid on state-action space.

Johri et al. proposed a neuro-dynamic programming (NDP) approach (Johri et al., 2011) (Johri et al., 2014) to the optimization of supervisory control for series hybrid hydraulic vehicle, considering the reduction of fuel consumption and pollutant emissions. The algorithm eliminates the requirement to loop over all possible states for calculating the exact cost-to-go value, and the computation load increases linearly with the number of parameters in the approximate function, rather than exponentially with number of states. The result shows the capacity of NDP algorithm to solve large problems and significant improvement on emission reduction.

1.3.2 Battery Aging Model

Lithium-ion battery is a promising candidate to provide the second energy source for HEV application. It has high volumetric and mass energy density, which is important for vehicle weight and volume. However, battery aging poses a challenge for practical applications. Complicated aging processes (Vetter et al., 2005) lead to either power fade or capacity fade that reduces battery performance. Models for battery aging are required to evaluate battery life under different control strategy. A significant number of papers have been focused on modeling battery aging. Based on the approaches reviewed in (Sauer et al., 2008), these models could be classified into Ah-throughput model and electrochemical model.

The Ah-throughput model is a semi-empirical model. It relates the accumulating lifetime reduction with the energy charge passing through battery cell, which is counted by ampere hour (Ah). Under standard lab conditions, battery life reduction is equal to the physical Ah throughput. Real-world operating conditions usually deviate from standard condition, and it either increases or decreases battery life. The impact of operating conditions on battery lifetime increase or decrease is described by a severity factor, and the battery life reduction is calculated by multiplying the severity factor with the physical Ah throughput. The severity factor is calculated by fitting experimental data.

Wang et al. (Wang et al., 2009) generated cycling induced capacity fade model of a $LiFePO_4$ battery that accounts for Ah throughput, C-rate, and temperature. The model was validated by a wide range of temperature (-30 to 60 °C), depth of discharge (90 to 10%), and C-rate (0.5C to 10C), and for each test, the cycling current is constant.

Todeschini et al. (Todeschini el al., 2012) proposed a capacity fade model of LiFePO4 battery that links C-rate and state of charge range. The modeled is validated using constant C-rate (2C to 8C) at fixed battery temperature of 55 °C. Onori el al. (Onori et al., 2012) proposed a capacity fading model of a $LiFePO_4$ battery for plug-in HEV (PHEV) application. The model relates aging with battery temperature and depth of discharge (DOD). Due to the low c-rate for PHEV application, the C-rate effect can be neglected. Cordoba-Arenas et al. (Cordoba-Arenas et al., 2015) proposed a capacity and power fade model of Li-ion pouch cells with NMC-LMO positive electrodes for PHEV application. The model includes the influenced by the charge sustaining/depleting ratio, minimum SOC, charging rate and temperature. Suri et al. (Suri et al., 2016) proposed a capacity fade model of $LiFePO_4$ battery related with current, temperature, and state of charge.

The Ah-throughput model has advantages of high computational speed and ease of implementation. It is usually coupled with the equivalent circuit model for system-level study. Hence it is very useful for the analysis and design of large systems in a short time. However, it requires large amount of lifetime measurements, and cannot predict aging effects based on electrochemical analysis.

The second category is electrochemistry-based model, with detailed description of chemical reaction kinetics, mass conservation, and mass diffusion. The most established mathematical description of batteries with porous electrodes has been developed by Newman et al. (Newman et al., 2004) using both concentrated solution theory and porous electrode theory. Based on the spatial resolution, the electrochemistry based models can be classified into single particle model (Safari et al., 2009) (Guo et al., 2011) (Ning et al.,

2004) and pseudo two-dimensional model (P2D model) (Ramadass et al., 2004) (Cai et al., 2013) (Lin et al., 2013). In the single particle model, each electrode is simplified into a single electrode particle, and it considers the lithium ion diffusion in the radial direction within each electrode particle. The concentration along electrode is assumed uniformly distributed, and the electrolyte concentration is assumed constant. In the P2D model, each electrode is modeled as a matrix of particles. The local concentration along electrode is calculated, and the variance of electrolyte phase concentration is considered.

Battery aging is complex, which is caused by many different processes and their interactions, for example, electrolyte decomposition, contact loss of active material, and metallic lithium plating. Darling et al (Darling et al., 1998) proposed a P2D model of Graphite-$Li_xMn_2O_4$ battery by integrating the side reaction kinetics of solvent oxidation into the intercalation reaction. It enables predicting the influence of side reactions on the current-potential behavior. Christensen et al. (Christensen et al., 2004) proposed a model of the solid electrolyte interphase (SEI) for aging. It can be used to estimate the SEI film growth rate, film resistance, and the irreversible capacity loss during cycling. Ploehn et al. (Ploehn et al., 2004) proposed a solvent diffusion model to predict the capacity loss during storage under constant potentials. Ramadass et al. (Ramadass et al., 2004) developed a capacity fade model by incorporating solvent reduction reaction at negative electrode into intercalation. The model is validated under constant current and constant voltage charging. Safari et al. (Safari et al., 2009) proposed a single particle model for the aging prediction of $LiCoO_2$/graphite battery. Solvent decomposition that lead to the growth of an SEI film is considered as the aging mechanism. Except for the decomposition kinetics, solvent diffusion through the SEI film is also considered. The model enables the prediction of both capacity fade and the increase of SEI resistance in different operation modes, namely charge/discharge cycling, constant-voltage, and OCV storage. Prada et al. (Prada et al., 2013) proposed a capacity and power fade model of $LiFePO_4$-graphite battery that due to SEI growth. The model is validated using dynamic current cycles under different temperature.

Electrochemical models have larger computation requirement comparing with Ah-throughput model. Ramadesigan et al. (Ramadesigan et al., 2012) shows the tradeoff between computation loads with battery model predictability. Although electrochemical-based model requires a significant computation effort, using it is very attractive due to the fidelity.

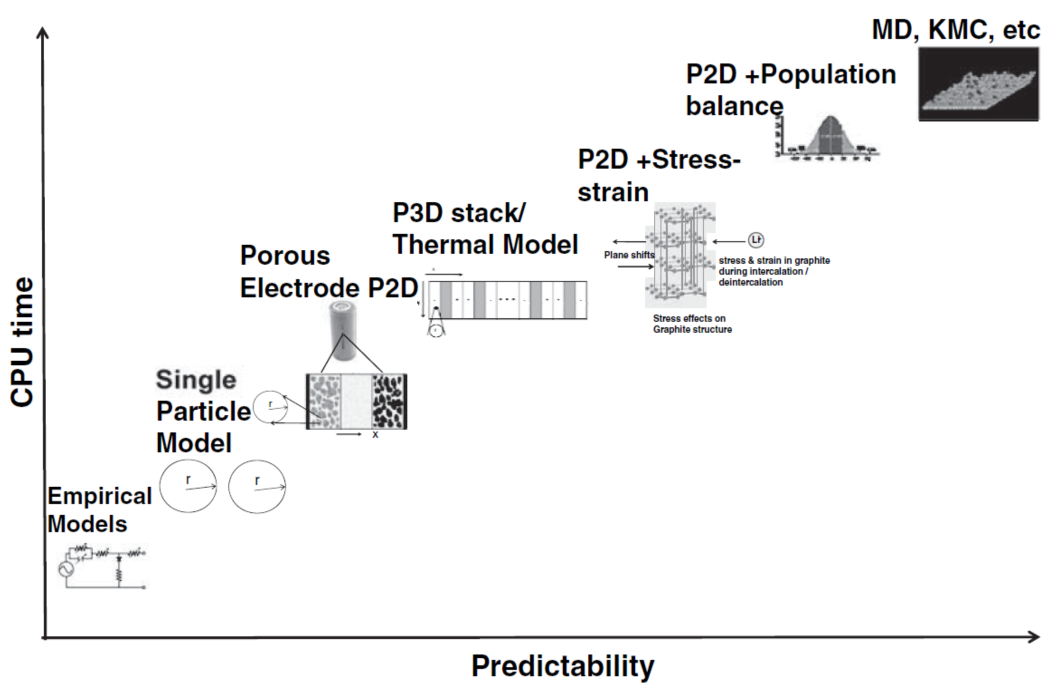

Figure 1.5: Computation demands of battery modeling with different predictability (Ramadesigan et al., 2012)

Battery aging has been addressed in battery management system. Hu et al. (Hu et al., 2015) uses Ah-throughput aging model for battery charge control optimization. Moura et al. (Moura et al. 2012) and Dey et al. (Dey et al., 2014) use single particle model for state of health estimation.

Battery aging is also critical for system-level study. The aging model has been used for assessment of control strategies. The Ah-throughout aging model combined with equivalent circuit battery model (Serrao et al., 2011) (Ebbesen et al., 2011) (Ebbesen et al., 2012) (Sciarretta et al., 2014) (Li et al., 2014) has been studied for parallel HEVs including plug-ins, with considering c-rate or SOC. The electrochemical-based battery model was first integrated into plug-in HEV system by Moura et al. (Moura et al., 2013). In the power management optimization, battery aging model is simplified as a static process, and represented as a function of current and battery state of charge (SOC).

1.4 Technical Challenges

The design of supervisory controller for heavy-duty series hybrid electric military truck is particularly challenging for the following reasons:

1. In case of heavy off-road vehicles such as tactical trucks, battery thermal management has been identified as a critical issue with respect to vehicle endurance and reliability. Extreme environment conditions and aggressive load cycles mandates the application of refrigeration system to battery

cooling. This leads to high ancillary power. Hence the parasitic cooling loss needs to be addressed.

2. Other than fuel economy, battery life is another important attribute in the vehicle design. Heavily dynamic load cycles with elevated temperature accelerate battery aging; thus reducing vehicle performance, but also introducing the replacement cost. The operation conditions decided by the supervisory controller have large impact on battery life.
3. The hybrid electric powertrain is a complex system consisting of interactive components. Multiple vehicles attributes are required to improve simultaneously. A predictive simulation framework is needed for systematic screening of the optimization of the supervisory control for a choice of relevant objectives.
4. System analysis with objective of battery life increases simulation timescale. Model of aging rate needs high computational efficiency, and enables accurate prediction of the impact of operation conditions and thermal conditions on both system performance and battery life.
5. Inclusion of battery thermal management and aging in the supervisory controller design increases the number of states and control inputs. It challenges the optimization algorithms. Classical dynamic programming suffers from ‘curse of dimensionality’, and new algorithm is required to handle problems with large state-action space and multiple objectives.

1.5 Contributions

This dissertation develops a framework to design a supervisory controller for series hybrid electric vehicle through multi-variable, multi-objective optimization of the vehicle power system. The foundation is established with development of a unified, multiphysics hybrid electric vehicle simulation tool for heavy-duty medium trucks, and the proposed optimization algorithms enables the improvement of supervisory controller on both fuel economy and battery life. The main contributions of this study in the field of optimal control for hybrids are:

- Develop a high-fidelity and computational-efficient simulation tool for in-depth studies of series HEV system for a heavy vehicle
    1. Integrate a lumped-parameter thermal model and refrigerant-based cooling model into system model that enables the evaluation of battery temperature and auxiliary power consumption.
    2. Integrate electrochemical based aging model for Lithium-ion battery including the thermal effect on aging rate, and enable the prediction of both battery capacity fading and power fading
    3. Analyze the impact of battery side reaction and cooling loss on fuel efficiency and battery life
- Develop a framework to optimize the supervisory control of the vehicle power system
    1. Apply Stochastic Dynamic Programming (SDP) and generate real-time implementable control strategies for uncertain future driving missions.

2. Integrate power management and battery thermal management, and investigate the benefit of coordinating the power system and cooling system
3. Investigate the tradeoff between fuel economy and battery life
4. Implement battery aging model with enhanced prediction accuracy under dynamic load cycles for optimization procedure. Consider lithium ion diffusion to obtain better representation and explore techniques for improving computation speed
5. Demonstrate the optimization of S-HEV system supervisory control with large state-action space problem using Neuro Dynamic Programming (NDP).

1.6 Dissertation Overview

This dissertation is organized as follows. Chapter 2 introduces the powertrain configuration, component model, and system model integration. In chapter 3, a baseline control strategy with separated battery thermal management and power management is embedded into the supervisory controller, and the impact of battery cooling and side reaction on system performance is analyzed under different battery temperature. Chapter 4 applies stochastic dynamic programming to the optimization of supervisory control with integration of battery thermal management and battery aging. Chapter 5 proposes neuro dynamic programming algorithm, and demonstrates the efficient computation and improved result with increased number of states. Finally chapter 6 summarizes the main results of this dissertation and discusses possible future research directions.

CHAPTER TWO

SYSTEM SIMULATION FRAMEWORK FOR SERIES HEV

This chapter describes the high-fidelity system model used in this dissertation. It is built based on Simulink/AMESim co-simulation, and is used for systematic analysis and control strategy evaluation. The first section introduces the powertrain configuration for series hybrid electric vehicle. The second section describes models relevant to battery, including electrical model, aging model, thermal model, and cooling model. Next describes models of other components. The last section integrates component models into powertrain system.

2.1 Vehicle Configuration

This study focuses on series hybrid electric powertrain (HEV). Series HEVs have great benefit of reducing fuel consumption, improving packaging efficiency, extending silent operation, and onboard power (Khalil et al., 2009). Figure 2.1 shows the power flow diagram. The primary power source for vehicle traction is the power pack consisting of internal combustion engine coupled with generator; engine has no mechanical connection with wheels, and this brings full flexibility of engine operation control. Battery is integrated to provide bidirectional power flow, and the cooling system keeps the battery pack within desired temperature range. Four in-hub electric motors are incorporated into wheels and provide traction power exclusively. During braking, electric machines work as generators and convert braking power to electric power. All power flows are integrated via a powerbus. Supervisory controller aims to minimize the energy consumption by controlling the power flow in the powertrain system. It receives driver's command, and sends commands to all components based the embedded supervisory control strategy. Table 2.1 shows the vehicle specifications. The powertrain is designed to handle heavy-duty driving missions at 49ºC ambient temperature.

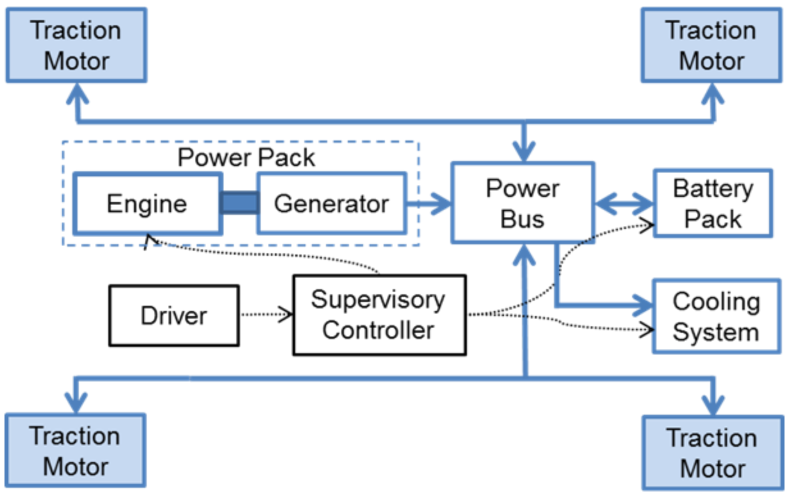

Figure 2.1: Series HEV powertrain configuration. Blue solid lines show the power flow, and black dot lines show the control signal flow.

Table 2.1: Series HEV Specifications

Component	Specification
Vehicle	Hybridized mid-size Truck
Vehicle Weight	14,000 kg
Frontal Area	5.72 (Width/Height: 2.49/2.7 m)
Engine	I8 Turbo-Diesel Engine: 330 kW
Generator	Permanent Magnet: 330 kW
Battery	$LiFePO_4$-Graphite battery Pack: 9 kWh
Motors	Permanent Magnet: 4*95kW (Continuous)

2.2 $LiFePO_4$/Graphite Battery Model

$LiFePO_4$/Graphite battery is a promising candidate of the bidirectional energy device for HEV application. The key advantages include high discharge rating, long cycle life, and excellent thermal and chemical stability.

Figure 2.2 illustrates the schematic diagram of a lithium-ion battery cell. It includes a negative electrode, separator, and a positive electrode. The negative electrode is composed by active materials of lithium carbon, and the positive is composed by lithium metal oxide. The separator separates two electrodes, and it avoids electrical short circuits. Electrodes and separator are porous, and the porosity is filled by electrolyte in liquid phase. It enables lithium ions (Li^+) to diffuse between electrodes. During discharging, Li^+ deintercalates from the negative electrode, migrate through electrolyte, and intercalates into the positive electrode. Correspondingly, electrons flows from the negative electrode to positive through external circuit. This is called intercalation process, and it is reversible reaction. During charge, Li^+ flows in the opposite direction.

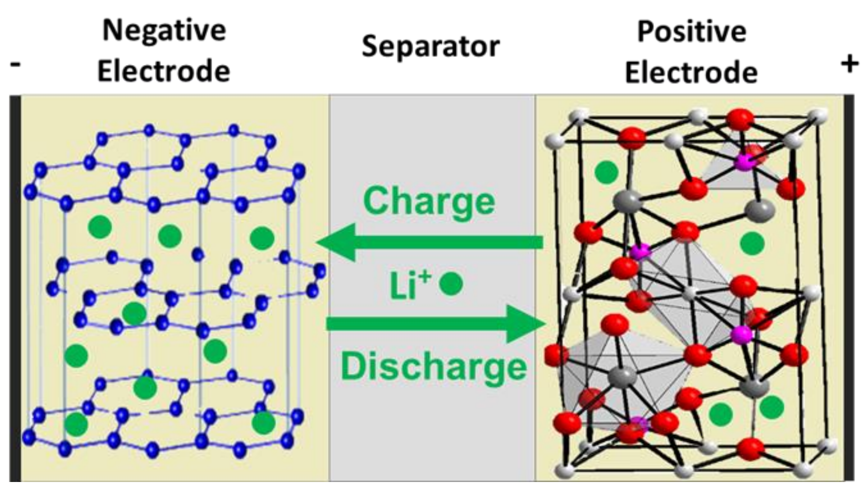

Figure2.2: Schematic diagram of a Li-ion battery cell

Along with intercalation process, side reactions take place in either electrode or electrolyte. It is irreversible reaction, and changes the structure of components and materials that degrades battery performance (Vetter et al., 2005). There are a multitude of aging mechanisms. In the case of Graphite-$LiFePO_4$ battery, one of the main aging mechanisms when cycling in the elevated temperature is associated with electrolyte decomposition. It is caused by electrolyte instability under the operation voltage of graphite anode. This process causes irreversible consumption of active lithium ions and leads to capacity fading. The decomposition products build a solid electrolyte interphase (SEI) film that covers the surface of negative electrode (Figure 2.3) (Vetter et al., 2005). It decreases the accessible active area and increases internal resistance, which is associated with power fading.

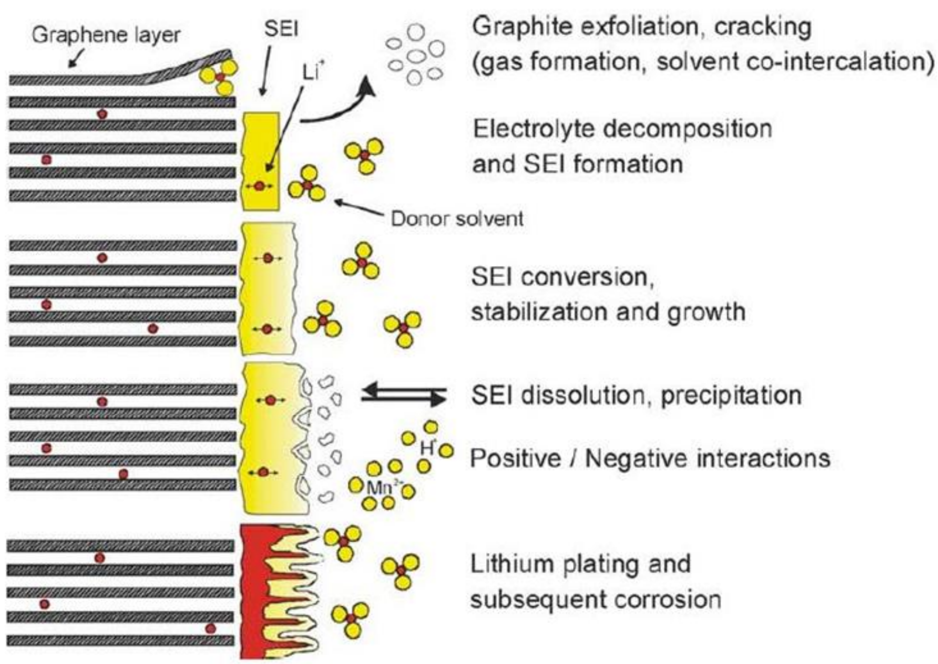

Figure 2.3 Growth of Solid Electrolyte Interphase Film at the anode/electrolyte interface (Vetter et al., 2005)

2.2.1 Model Equations for Side Reaction

A single-particle aging model of $LiFePO_4$-Graphite Li-Ion batteries (Prada et al., 2013) has been selected and integrated into vehicle powertrain system. Reductive electrolyte decomposition on negative electrode during charging is modeled as the major source of aging. It was validated predictions of the fading process with dynamic load cycle, and include thermal effect on battery performance (Prada et al., 2013). Hence it enables to quantitate the battery aging effect on HEV system. No side reaction is considered in positive electrode due to the stabilization of $LiFePO_4$ material.

The chemical equations for lithium ions intercalation are shown in Eq. 2.1 and 2.2 for positive electrode and negative electrode, respectively.

$$xLi^{+} + xe^{-} + Li_{1-x}FePO_4 \underset{Charge}{\overset{Discharge}{\rightleftarrows}} LiFePO_4 \tag{2.1}$$

$$LiC_6 \underset{Charge}{\overset{Discharge}{\rightleftarrows}} xLi^{+} + xe^{-} + Li_{1-x}C_4 \tag{2.2}$$

The reaction current density for lithium ion intercalation is described by Butler-Volmer equation:

$$i_{\mathrm{int,n}} = i_{0,\mathrm{n}}\{\exp(\frac{\alpha F}{RT}\eta_n^k) - \exp(-\frac{\alpha F}{RT}\eta_n^k)\}\exp(\frac{E_a}{R}(\frac{1}{T_{ref}} - \frac{1}{T_{bat}})) \tag{2.3}$$

where $i_{0,f}$ is the exchange current density and assumed as a constant. η_f^k is the kinetic overpotential, and describes as follows:

$$\eta_n^k = \phi_e - \phi_s - U_{n,ref} - \frac{i_t}{a_n}R_{film} \tag{2.4}$$

The electrolyte reduction is assumed to occur at the interface of negative electrode and electrolyte during charge. The reaction scheme is simplified into Eq. 2.5:

$$S + 2e^{-} + 2Li^{+} \xrightarrow{charge} P \tag{2.5}$$

where S represents solvent in electrolyte, e^- is electrons, Li^+ is Lithium ion, and P represents the reductive products that build SEI layer. And its reaction current density and overpotential is represented as:

$$i_s = -2Fk_f\, c^*_{solv} (c^s_{s,n})^2 \exp(-\frac{\alpha F}{RT}(\eta_s))\exp(\frac{E_a(\psi)}{R}(\frac{1}{T_{ref}} - \frac{1}{T_{bat}})) \tag{2.6}$$

$$\eta_s = \phi_e - \phi_s - U_s - \frac{i_t}{a_n} R_{film} \tag{2.7}$$

The thermal effect on reaction rate is included in Eq. 2.3 and 2.6 Arrhenius law. T_{ref} is the reference temperature, T_{bat} is battery temperature, and E_a is activation energy (J mol^{-1}).

The total current density for negative and positive electrode is represented by Eq. 2.8 and 2.9, respectively.

$$i_{t,n} = i_{int,n} + i_{s,n} \tag{2.8}$$

$$i_{t,p} = i_{int,p} \tag{2.9}$$

The current density is assumed to be uniformly distributed along electrode, so that:

$$i_t = \frac{I}{S_n} \tag{2.10}$$

where I is battery current, and S_n is the electroactive surface of electrode.

The porous electrode is represented by a single spherical particle, and lithium ions diffuses inside of particle. Following Fick's laws of diffusion, the local concentration of

Li^+ inside of particle are calculated by Eq. 15. At the particle center, the diffusion is considered as symmetrical, which shows in Eq. 16. At the particle surface, the boundary condition is impacted by local current density, as shown in Eq. 17.

$$\frac{\partial}{\partial t}c_s - \frac{1}{r^2}\frac{\partial}{\partial r}(\mathrm{r}^2\mathrm{D_s}\frac{\partial}{\partial r}c_s) = 0 \tag{2.11}$$

$$\mathrm{D_s}\frac{\partial}{\partial r}c_s\bigg|_{r=0} = 0 \tag{2.12}$$

$$-\mathrm{D_s}\frac{\partial}{\partial r}c_s\bigg|_{r=R_s} = \frac{i_{\mathrm{int}}}{F} \tag{2.13}$$

The lithium ion concentration in electrolyte phase is assumed constant in this study.

The reductive electrolyte decomposition lead to two fading mechanisms: 1) capacity fading due to irreversible Li-ion consumption, 2) power fading due to the reduction of electrode porosity and increase of SEI film resistance.

The variation of irreversible lithium ion loss can be expressed as Eq. 2.14.

$$\frac{d}{dt}Q_s = S_n i_s \tag{2.14}$$

where S_n is the electroactive surface of the negative electrode.

The SEI film increases with the growth rate as follows:

$$\frac{d}{dt}\delta_{SEI} = -\frac{M_{SEI}}{2F\rho_{SEI}}i_s \tag{2.15}$$

And the resistance increase of the SEI film is described as:

$$\frac{d}{dt}R_{SEI} = -\frac{M_{SEI}}{2\kappa_{SEI}S_nF\rho_{SEI}}i_s \tag{2.16}$$

The SEI film penetrates in the porosity of negative electrode, and available volume fraction of electrolyte decreases as follows:

$$\frac{d}{dt}\varepsilon_{e,n} = \frac{3M_{SEI}\varepsilon_{e,n}}{2F\rho_{SEI}R_{s,n}} i_s \tag{2.17}$$

The internal resistance increases with SEI film growth, as shown in Eq. 2.18.

$$R = \frac{\varepsilon_{SEI}}{k_{SEI}S_n} + \frac{1}{2A}\left(\frac{\delta_n}{\kappa\varepsilon_{\mathrm{e},n}{}^{\mathrm{Brugg,n}}} + 2\frac{\delta_{sep}}{\kappa\varepsilon_{\mathrm{e,sep}}{}^{\mathrm{Brugg,n}}} + \frac{\delta_p}{\kappa\varepsilon_{\mathrm{e,p}}{}^{\mathrm{Brugg,n}}}\right) \tag{2.18}$$

where S_n is the electroactive surface of the negative electrode, M_{SEI} is SEI layer molar mass, ρ_{SEI} is SEI layer density, κ_{SEI} is the SEI ionic conductivity, and F is Faraday's constant. The increase of SEI resistance is added into battery internal resistance.

The voltage is calculated by:

$$V = U_p\left(\frac{c^s_{s,p}}{c^s_{s,p,\max}}\right) - U_n\left(\frac{c^s_{s,\mathrm{n}}}{c^s_{s,\mathrm{n},\max}}\right) + \eta^k_n - \eta^k_p - IR \tag{2.19}$$

This battery model is able to predict the fading process with dynamic load cycle (Prada et al., 2013), and hence enables accurate prediction of battery fading with the command from series HEV supervisory control.

2.2.2 Solution for Lithium Ion Concentration in Spherical Particle

The lithium ion concentration at the electrode surface is an important factor to determine reaction kinetics. The intercalation or deintercalation process at electrolyte/electrode interface causes Li^+ diffusion inside of electrode, and the Li^+ concentration is not uniformly distributed as shown in Figure 2.4. Figure 2.5 compares the electrode surface Li^+ concentration with average Li^+ concentration, using dynamic current profile from HEV simulation under urban drive. The average concentration fails to capture the peaks and dynamics of surface concentration. Hence the sum of side reaction rate per cycle is 9.4% higher than the prediction with average concentration.

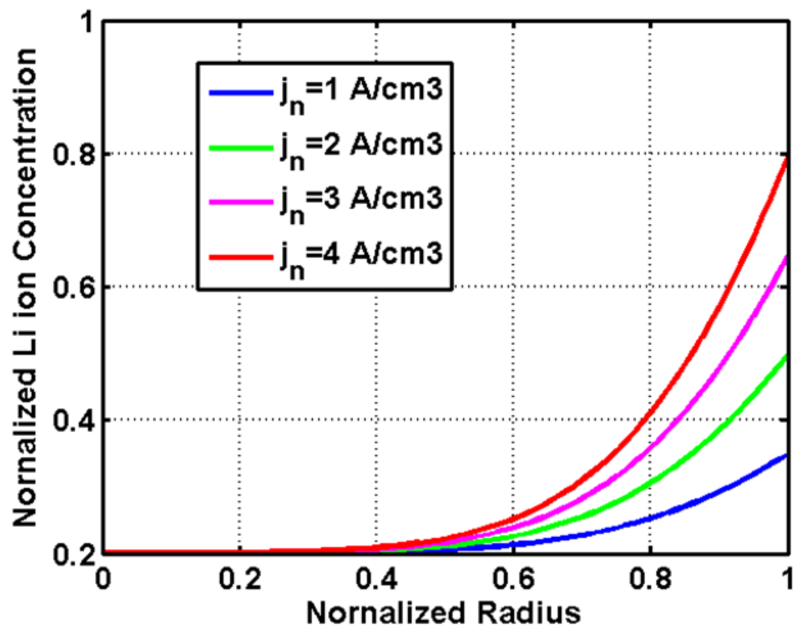

Figure 2.4: The distribution of Li ion concentration in electrode with variation of current density j_n

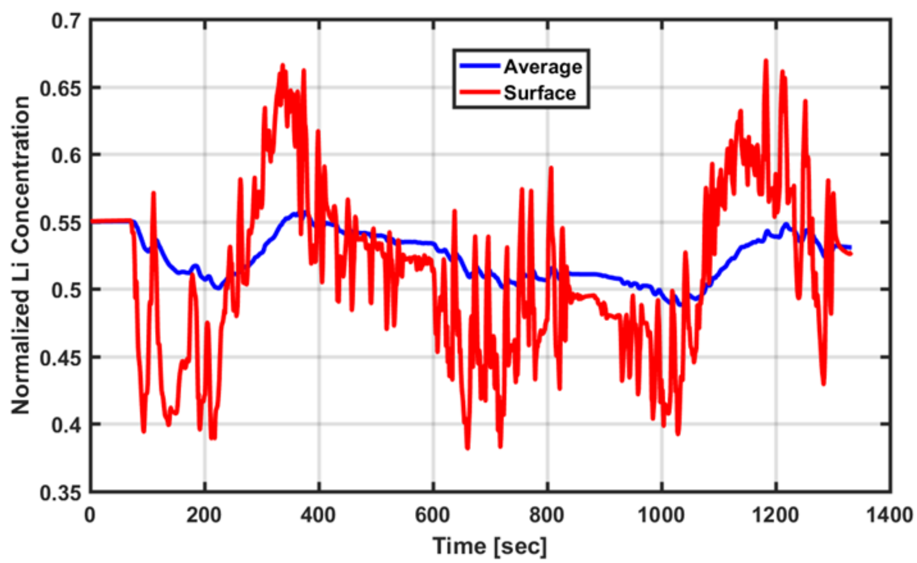

Figure 2.5: Compare Surface Li^+ concentration with average concentration of electrode.

To calculate the Li^+ surface concentration and hence to determine the side reaction rate, the partial differential equations (Eq. 2.11-2.13) described by Fick's laws of diffusion is required to solve along the radius dimension of spherical particle.

There are several discretization methods to compute the diffusion equations (Rahn et al., 2013). For example, the finite difference method (FDM) discretizes the particle radius into grids, and the partial differential equation (PDE) is reduced to ordinary differential equations (ODE) that needs to solve at each grid point. However, it requires long simulation time with a large number of ODEs to solve. The HEV powertrain model includes multiple variables from each components, and systematic analysis of vehicle performance with prediction of battery life requires simulation under years of usage. A battery aging model with computational efficiency is required for integration into the vehicle simulation framework.

Hence an approximate analytical solution (Guo et al., 2012) for spherical diffusion equations is adopted to compute the Li^+ surface concentration, instead of calculating the whole distribution inside of electrode.

The diffusion equations (Eq. 2.11-2.13) can be rewritten in the dimensionless form by choosing the dimensionless variables are defined as follows:

$$C = \frac{c_{Li^+}}{c_{\max}} \tag{2.20}$$

$$\tau = \frac{D_s t}{R^2} \tag{2.21}$$

$$\delta(\tau) = \frac{i_t(\mathrm{t})\mathrm{a_s R}}{D_s c_{\max}} \tag{2.22}$$

$$\bar{r} = \frac{r}{R} \tag{2.23}$$

where c_{max} is the maximum Li^+ concentration in the particle, t is time, R is particle radius, i_t is the local reaction rate which is treated as boundary flux.

Then the dimensionless analytical solution of lithium ion concentration at the particle surface contains the average concentration plus an infinite series of eigenfunction, and could be written as:

$$C_s(\tau) = \overline{\mathrm{C}}(\tau) + \sum_{n=1}^{\infty} Q_n(\tau) \tag{2.24}$$

where $\bar{C}$ is the average Li^+ volumetric concentration and is determined by

$$\frac{d\overline{C}}{d\tau} = -3\delta(\tau) \tag{2.25}$$

with initial condition:

$$\overline{C}(\tau = 0) = C_0 \tag{2.26}$$

The variation of Q_n is defined as:

$$\frac{dQ_n}{d\tau} = -\lambda_n^2 Q_n(\tau) - 2\delta(\tau) \tag{2.27}$$

$$Q_n(\tau = 0) = 0 \tag{2.28}$$

where λ_n is the nth eigenvalue calculated from the following equation:

$$\lambda_n - \tan\lambda_n = 0 \tag{2.29}$$

To calculate the value of surface concentration, the infinite series of eigenfunction is truncated by N terms, and the following terms is replaced by truncation error, $e_N^{apx}(\tau)$ and defined as:

$$e_N^{apx}(\tau) = -2\delta(\tau)\{(\frac{1}{10} - \sum_{n=1}^{N}\frac{1}{\lambda_n^2})[1-\exp(-\lambda_{N+1}^2\tau)] + \sqrt{\frac{\tau}{\pi}}\operatorname{erfc}(\lambda_{N+1}\sqrt{\tau})\} \qquad (2.30)$$

Then the approximate solution of surface concentration could be rewritten as

$$C_s^{apx}(\tau) = \overline{C}(\tau) + \sum_{n=1}^{N} Q_n(\tau) + e_N^{apx}(\tau) \qquad (2.31)$$

To select the number N, the approximate solution with different N values are compared with FDM solution (Beers et al., 2007). The r dimension along electrode particle is discretized into M intervals with M-1 internal nodes, and the ordinary differential equation at mth node is described as:

$$-\frac{m+1}{m}\frac{Ds}{\Delta r^2}c_{s,m+1}^{t+\Delta t} + (\frac{2Ds}{\Delta r^2} + \frac{1}{\Delta t})c_{s,m}^{t+\Delta t} - \frac{m-1}{m}\frac{Ds}{\Delta r^2}c_{s,m-1}^{t+\Delta t} = \frac{1}{\Delta t}c_{s,m}^{t} \qquad (2.32)$$

where m=1,2,…,M-1, and $\Delta r = \frac{R}{M}$ is the length of interval.

The boundary condition at the particle surface (Mth node) can be expressed as:

$$\frac{dc_{s,\mathrm{M}}}{dt} = \frac{M-1}{M}\frac{Ds}{\Delta r^2}c_{s,\mathrm{m-1}} - \frac{M-1}{M}\frac{Ds}{\Delta r^2}c_{s,\mathrm{M}} - \frac{M+1}{M}\frac{1}{Fa_s\Delta r}j^{Li} \qquad (2.33)$$

Then the Li+ concentration at each node could be obtained by solving a set of linear equations.

Battery aging model solved by these two methods are integrated into series HEV simulation framework, respectively. Figure 2.6 shows the battery model input of current profile under urban driving condition. The node M in FDM is selected as 84. As shown in

Figure 2.7, the prediction accuracy of approximate analytical method improves by increasing the value of N. When N increases to six, the approximate analytic solution get close to FDM solution.

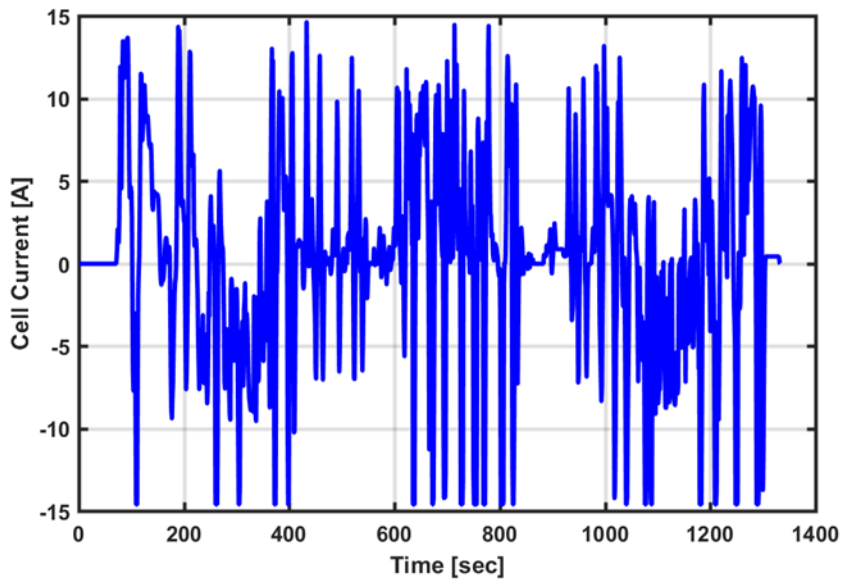

Figure 2.6: Cell current profile from thermostatic SOC control strategy with Assault driving cycle

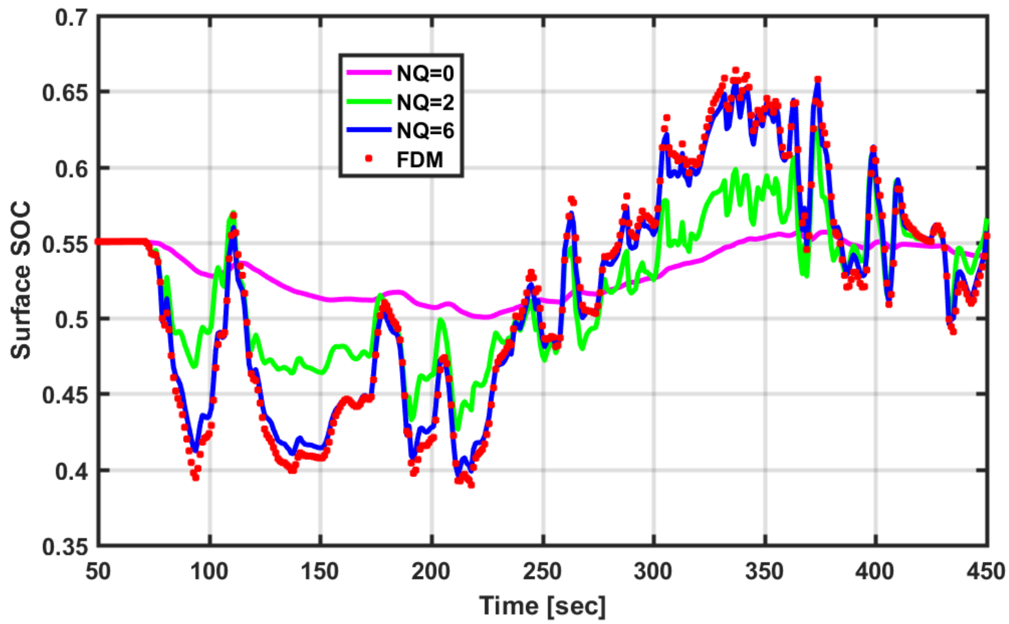

Figure 2.7: Compare approximate solution with finite difference method under Urban Assault Driving Cycle

Table 2.2 compares the computation time for 10-cycle simulation of basic equivalent circuit model (ECM), single-particle (SP) aging model with approximate analytical solution (N=6), and single-particle aging model with implicit FDM solution. It can been seen that the approximate analytical solution could largely improve computation speed comparing with FDM method. This makes the electrochemical based aging model as a promising candidate for system-level simulation with long timescale simulation.

Table 2.2 Compare computation time of vehicle system model with integration of different battery models

Model	ECM	SP Model with analytical solution	SP Model with FDM solution
Simulation Time [sec]	0.40	0.73	18.39

2.3 Battery thermal and cooling model

In case of heavy off-road vehicles such as tactical trucks, battery thermal management has been identified as a critical issue with respect to vehicle endurance and reliability. Battery generates significant amounts of heat under aggressive duty cycles mainly due to its internal resistance. The heat accumulation can cause a rapid increase of temperature in battery core; as a minimum this accelerates battery aging, but in the extreme it will lead to thermal runaway that may cause the battery cell to catch fire or to explode. Certain amount of power is required to remove heat from the battery pack, and since recommended safe temperature for the Li-Ion is only 55 ^{o}C. The ancillary loss can be quite high for extremely hot ambient conditions. In order to capture the effect of battery cooling system on both fuel economy and battery life, a lumped battery thermal model and refrigeration cooling system is modeled and integrated into vehicle system.

The mechanism of battery heat generation and cooling model is illustrated in Figure 2.8. Cylindrical battery's thermal behavior is modeled with two states (core temperature T_c and surface temperature T_s) (Forgez et al., 2010). Heat (Q_1) is generated in battery core, transferred to the surface, and rejected into the recirculating cooling air. Then the heated cooling air and coolant exchange heat in the evaporator.

The heat generation is described as:

$$Q_1 = I^2 R \tag{2.34}$$

where I is current and R is internal resistance.

The state dynamics of battery core temperature (T_c), surface temperature (T_s), and cooling air temperature (T_f) is described as:

$$C_c \frac{dT_c}{dt} = Q_1 + \frac{T_s - T_c}{R_c} \tag{2.35}$$

$$C_s \frac{dT_s}{dt} = \frac{T_f - T_s}{R_u} - \frac{T_s - T_c}{R_c} \tag{2.36}$$

$$C_f \frac{dT_f}{dt} = \frac{T_s - T_f}{R_u} - \dot{m}_{air} c_f (T_f - T_{f,in}) \tag{2.37}$$

where C_c, C_s, and C_f is the heat capacity, R_c, R_s, and $R_f$is thermal resistance, $\dot{m}_{air}$is the cooling air mass flow rate.

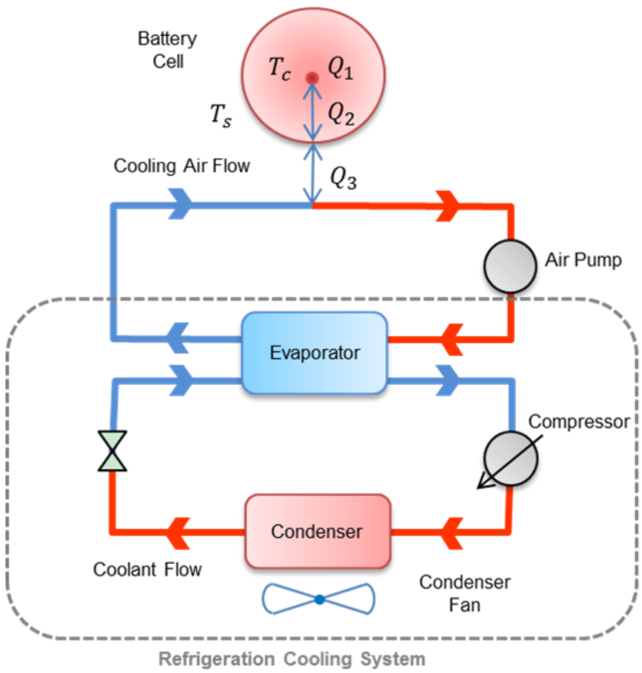

Figure 2.8: Battery thermal management system structure.

The refrigerant cooling system is built using AMESim shown in Figure 2.9. The system contains a compressor, a condenser, a throttle value, and an evaporator. It removes heat from cooling air that flows out from battery pack, and expel the heat into surrounding, using the refrigeration cycle of compression, condensation, expansion, and evaporation (Moran et al., 2010). In the cooling system, the compressor and air cooling fan consumes power.

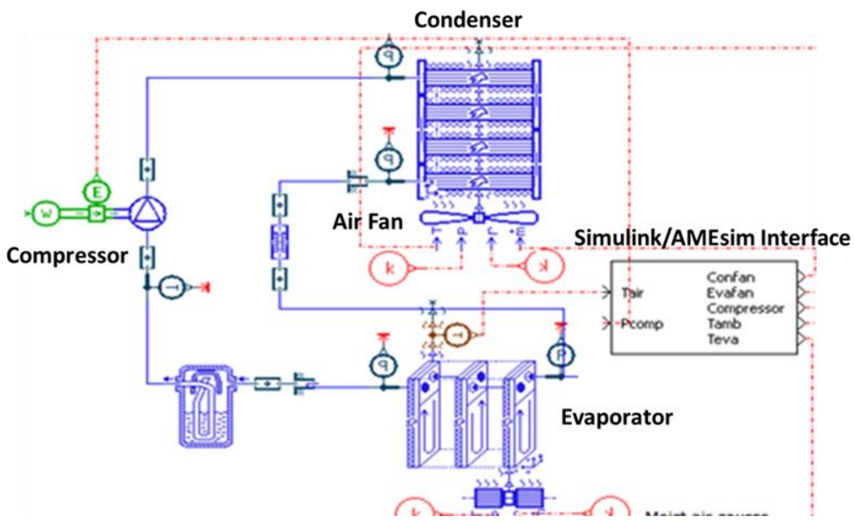

Figure 2.9: Refrigeration Cooling System constructed in AMESim (Tao et al., 2014)

2.4 Models for other components

2.4.1Power Pack

The power pack model inputs are the command from supervisory controller and the external load torque. As shown in Figure 2.10, the engine fuel-injection controller decides the command of fuel injection rate ($\dot{m}_f$), which has the inputs of desired engine torque ($T_{e,des}$) and speed ($\omega_{e,des}$) from supervisory controller. Then actual engine actual torque is calculated using a lookup table with fuel injection rate ($\dot{m}_f$) and engine actual speed (ω_e).

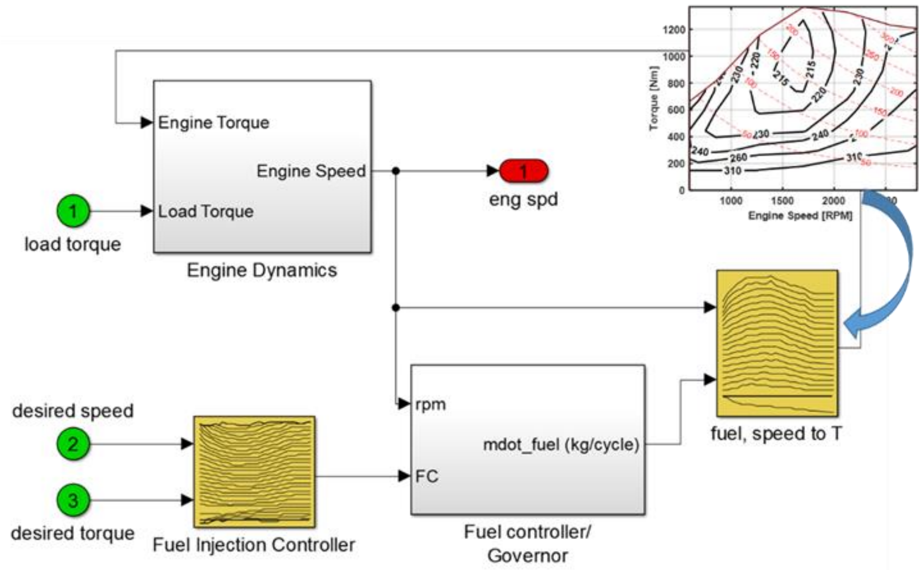

Figure 2.10: Diesel engine model in Simulink

The dynamics of engine rotation speed is calculated by:

$$(J_e + J_g)\frac{d\omega_e}{dt} = T_e - T_g \tag{2.38}$$

where J_e and J_g are the rotational inertia of engine and generator, and T_e and T_g are the engine torque and generator torque, respectively.

The generator speed (ω_g) is the same with engine, and the generator output electric torque is calculated by:

$$T_g = T_e \eta_g \tag{2.39}$$

where η_g is generator efficiency calculated by a quasi-steady state efficiency map.

The electric output power from the power pack is calculated by:

$$P_p = T_g \omega_g \tag{2.40}$$

2.4.2 E-Motors

The four e-motors are incorporated into the hub of wheels. The model built in Simulink is shown in Figure 2.11. The motor rotational speed ω_m is related with vehicle speed (V_{veh}) by:

$$\omega_m = \frac{V_{veh} g_{FD}}{R_{tire}} \quad (2.41)$$

where R_{tire} is wheel radius, and $g_{FD}$is the final drive gear ratio.

The output mechanism power ($P_{m,mech}$) to wheels is calculated by:

$$P_{m,mech} = P_{m,elec}\eta_m(P_{m,elec} \geq 0) + P_{m,elec} / \eta_m(P_{m,elec} < 0) \quad (2.42)$$

where $P_{m,elec}$ is the electric power from powerbus, and η_m is the efficiency related with motor rotational speed and torque. During vehicle braking ($P_{m,elec} < 0$), the e-motors act as generators, and convert the mechanism power from wheels to electric power.

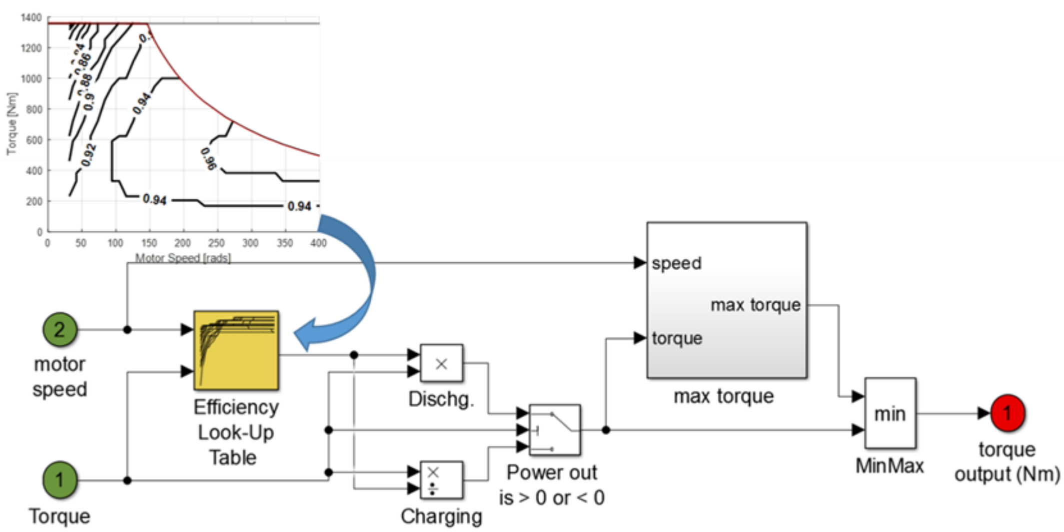

Figure 2.11: E-Motor Model in Simulink

2.4.3 Vehicle dynamics

The longitudinal dynamics of vehicle is calculated as:

$$M_v \frac{dV_{veh}}{dt} = F_t - (F_a + F_r + F_g + F_b) \tag{2.43}$$

where M_v is vehicle mass. F_t is the traction force, F_a is aerodynamic friction, F_r is rolling friction, F_g is the uphill driving force, F_b is the braking force. They are defined as follows:

$$F_t = \frac{P_{m,mech}}{V_{veh}} \tag{2.44}$$

$$F_a = \frac{1}{2}\rho_a A_f c_d V_{veh}{}^2 \tag{2.45}$$

$$F_r = c_r M_v g \cos(\alpha), \mathrm{V_{veh}} > 0 \tag{2.46}$$

$$F_g = M_v g \sin(\alpha) \tag{2.47}$$

where ρ_a is the air density, A_f the vehicle frontal area, c_d the aerodynamic drag coefficient, c_r the rolling friction coefficient, and α the road grade. Case studies developed in this dissertation consider the road grade to be zero.

2.5 System Integration

The key components and their subsystems are integrated into a complete vehicle powertrain system model, as shown in figure 2.12. The system model includes vehicle dynamics, driver, power pack (a diesel engine mechanically coupled with a generator), Li-ion battery and its cooling system, and four in-hub e-motors. The simulation framework is established using Matlab/Simulink. The refrigeration cooling system is built using Amesim and embedded into Simulink model through Simulink/Amesim interface. The power flows need to satisfy:

$$P_g + P_b = P_{comp} + P_{fan} + P_{m,elec} \tag{2.48}$$

This integrated simulation framework enables prediction of: (i) auxiliary power consumption under a variety of battery cooling load, (ii) side reaction of electrolyte decomposition with thermal effect, and (iii) the interaction with components. It has two functions in this dissertation. First is to predict fuel efficiency and battery life under different driving conditions, and to analyze the impact of cooling loss and side reaction on system efficiency in next chapter. Second is to evaluate the supervisory control strategies that proposed in Chapter Four and Chapter Five, and to demonstrate the improvement by optimization algorithm.

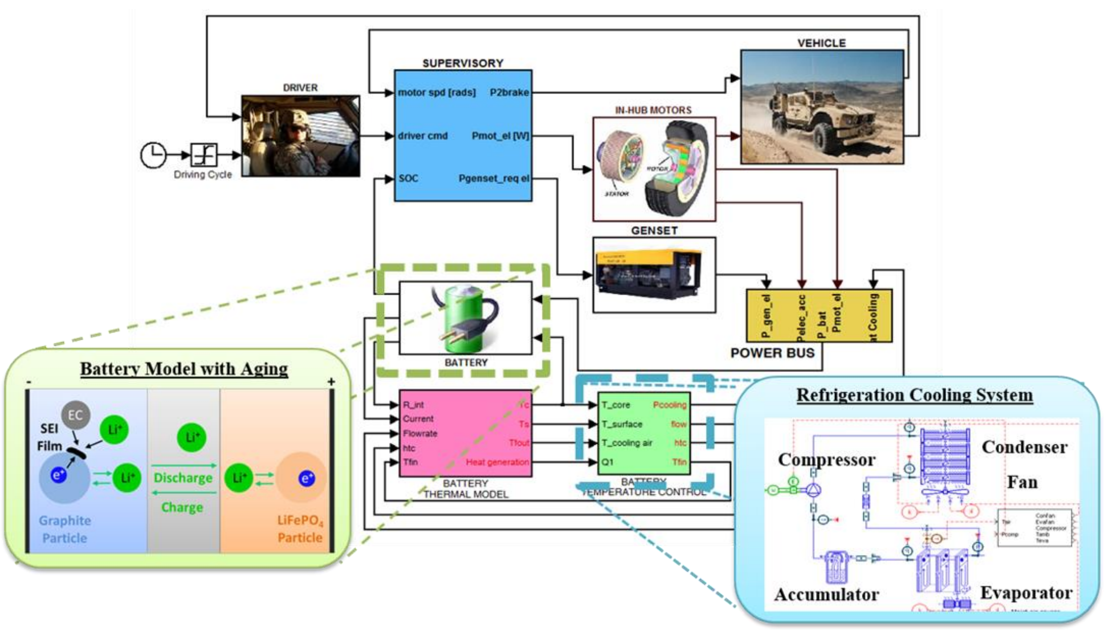

Figure 2.12: Integrated S-HEV Powertrain System Simulation Framework

CHAPTER THREE

THE IMPACT OF BATTERY THERMAL MANAGEMENT AND SIDE REACTION OF ELECTROLYTE DECOMPOSITION ON SYSTEM PERFORMANCE

This chapter studies the impact of battery cooling and side reaction of electrolyte decomposition on fuel efficiency and battery life. A baseline control strategy is embedded into the supervisory controller with separated power management and battery thermal management module. Several cases are analyzed with a wide range of battery temperature and different driving cycles. Each case study includes short-term and long-term simulation. In the short-term simulation, battery cells are assumed fresh, and it focuses the impact of battery cooling loss on system efficiency. In the long-term simulation, the side reaction of electrolyte decomposition is additionally considered, and its impact on both fuel economy and battery life is analyzed under different battery temperature.

This chapter is organized as follows. The first section describes the baseline control strategy for power management and battery thermal management. The second part shows short-term simulation results, and the third part is long-term simulation results. This chapter ends with summary.

3.1 Baseline Control Strategy

In the baseline control strategy, the power management and thermal management are designed separately, with target of SOC sustaining and battery temperature sustaining, respectively.

Thermostatic SOC control strategy is a typical heuristic power management strategy for S-HEVs (Kim et al., 2007) (Johri et al., 2009). It is robust and effective in sustaining battery state of charge (SOC), and it is combined with rules that keep engine/generator operation on the best efficiency line.

Figure 3.1 shows the thermostatic control logic: the power command is the desired electric power output of the engine-generator power pack; it is a function of battery state of charge (SOC). When SOC decreases below the low threshold (Target SOC), threshold power command is sent to the power-pack to prevent further SOC drop. If the vehicle power demand is higher and the SOC keeps dropping below $SOC_{threshold}$ the engine power command linearly increases up to the maximum output power. As SOC restores and rises above the high threshold (Target SOC+Deadband), engine is turned off or commanded to idle. The dead band is designed to avoid frequent engine shut-downs when power demand is fluctuating. To protect battery health, engine also turns on whenever the vehicle power demand exceeds battery discharging limit. And engine is set as idle if vehicle is braking and SOC does not exceed the maximum limit.

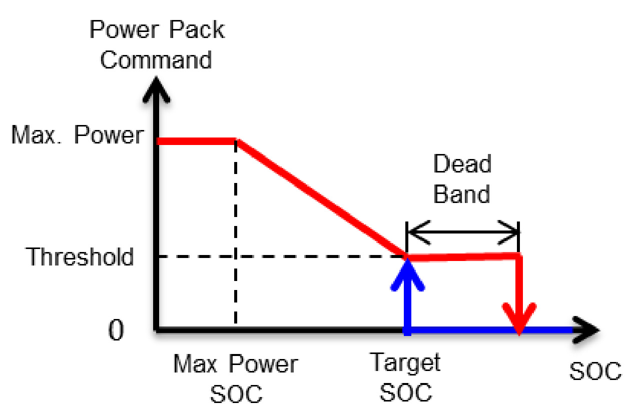

Figure 3.1: Thermostatic SOC control strategy.

The power-pack desired operation points are determined by the analysis of combined BSFC map (shown in Figure 3.2). Black solid isocontours show the combined BSFC, blue dash curve shows power level of power pack output, and the red solid line shows optimal combined BSFC for each output power.

Combined BSFC is defined in Eq. 3.1; it combines the engine fuel efficiency and generator efficiency (η_g).

$$BSFC_{comb} = \frac{\dot{m}_{fuel}(g/h)}{P_e(kW)\cdot\eta_g} \tag{3.1}$$

where P_e is engine power and $\dot{m}_{fuel}$ is the fuel rate.

The optimal combined BSFC line is the operation with the minimum fuel consumption for desired output electric power. It is generated by connecting points of minimum combined BSFC for any power level. Engine command is inferred from the SOC control logic illustrated in Figure 3.1. Engine speed (ω) and torque (T_e) is determined from the crossing of power command line and optimal combined BSFC line in Figure 3.2. The red point and dash line illustrate the engine operation at 150kW engine power. Thermostatic SOC strategy

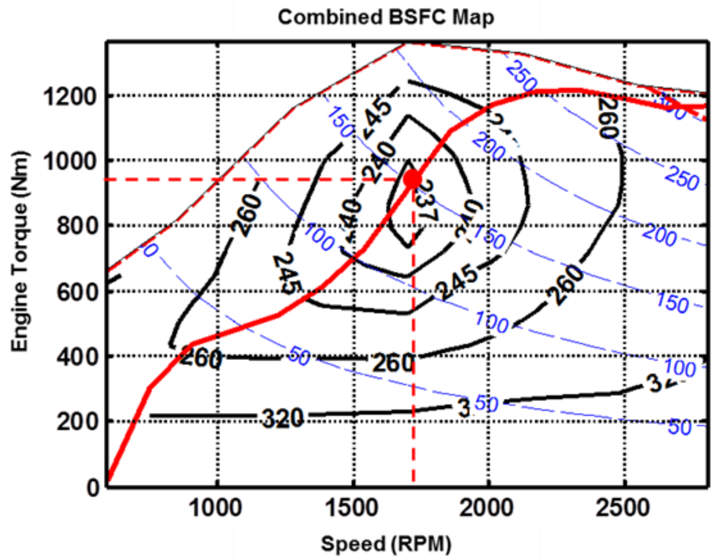

Figure 3.2: Combined BSFC Map.

The cooling system is controlled by a model predictive controller designed by Tao et al. (Tao et al., 2014). The controller tracks the cooling air temperature, and gives power command to the compressor unit. This controller is designed based on given battery duty cycle from Thermostatic SOC strategy. The cost function considers the battery core temperature stability and temperature magnitude inside of battery cell.

3.2 Short-term simulation – consideration of battery thermal management

This section studies the impact of battery temperature on system efficiency using short-term simulation. Battery cells are assumed in fresh condition. Two driving cycles are simulated, namely Urban Assault Cycle (Figure 3.3) and Convoy Cycle (Figure 3.4), and the target of battery average temperature (T_{bat}) varies from 20°C to 50°C with step size of 10°C. The ambient temperature is set as 49°C.

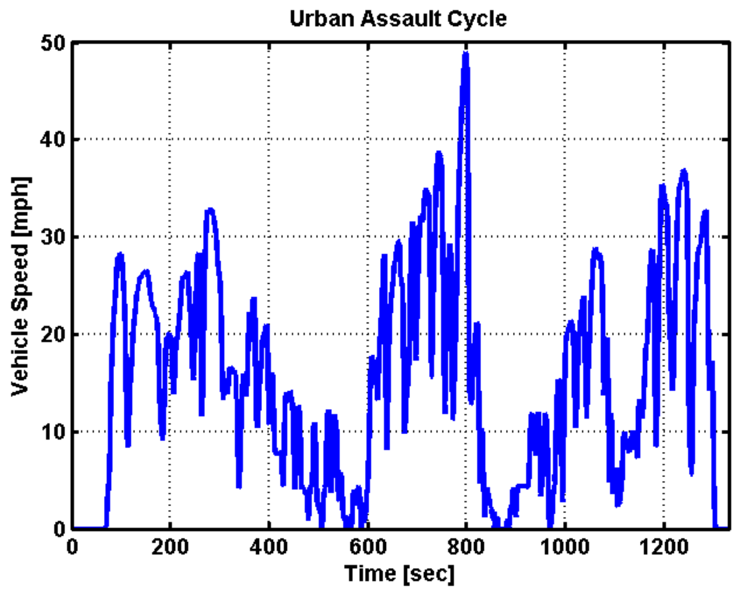

Figure 3.3: Speed profile of Urban Assault Cycle.

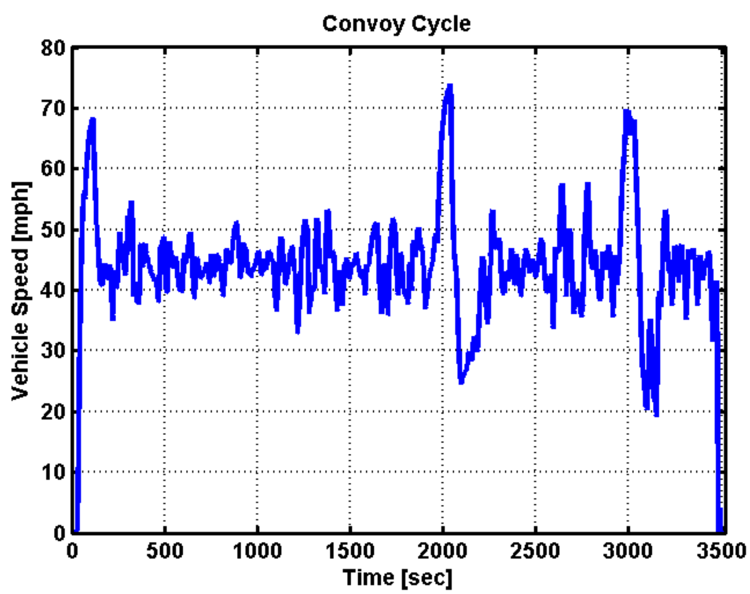

Figure 3.4: Speed profile of Convoy Cycle.

Figure 3.5 plots the MPG under different simulation cases. The blue lines are results considering the total power requirement of cooling and propulsion, and the red lines only considering vehicle propulsion. The difference between red and blue lines shows that there exists MPG loss due to battery cooling consumption. For the case of Assault Cycle with battery temperature of 30°C, the heat generation rate of battery pack can be above 10 kW (as shown in figure 3.6), and the maximum cooling power increases up to 4.1 kW, which is high enough to cause a 4.8% fuel economy loss.

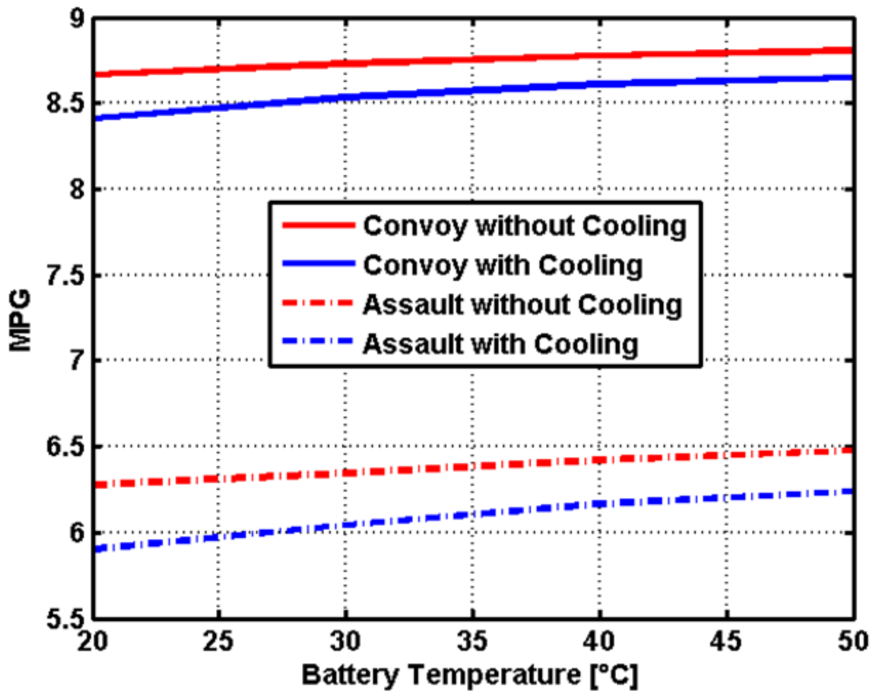

Figure 3.5: Compare MPG result under difference case studies

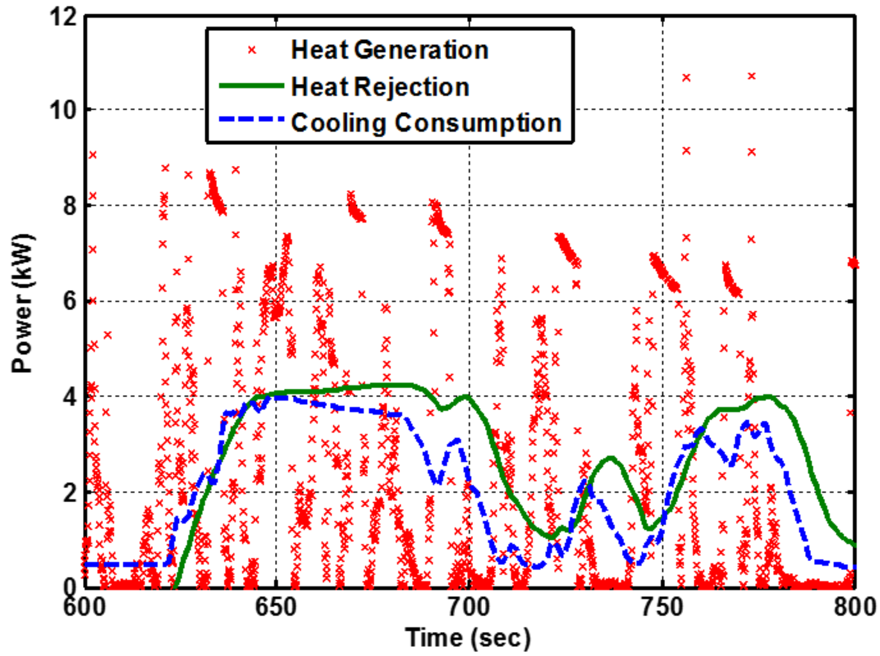

Figure 3.6: Battery heat generation and cooling consumption with Thermostatic SOC strategy over Assault Urban Cycle.

From Figure 3.7, we could also see that MPG drops with battery temperature. Two factors cause it. First is battery efficiency loss due to the increase of internal resistance (as shown in figure 3.8). This lead to MPG drop (blue lines) with temperature even without considering cooling consumption. The second is the increase of cooling penalty on fuel economy, as shown in figure 16. This penalty is smaller for convoy cycle than with assault, due to its smaller power ratio of cooling to vehicle propulsion larger.

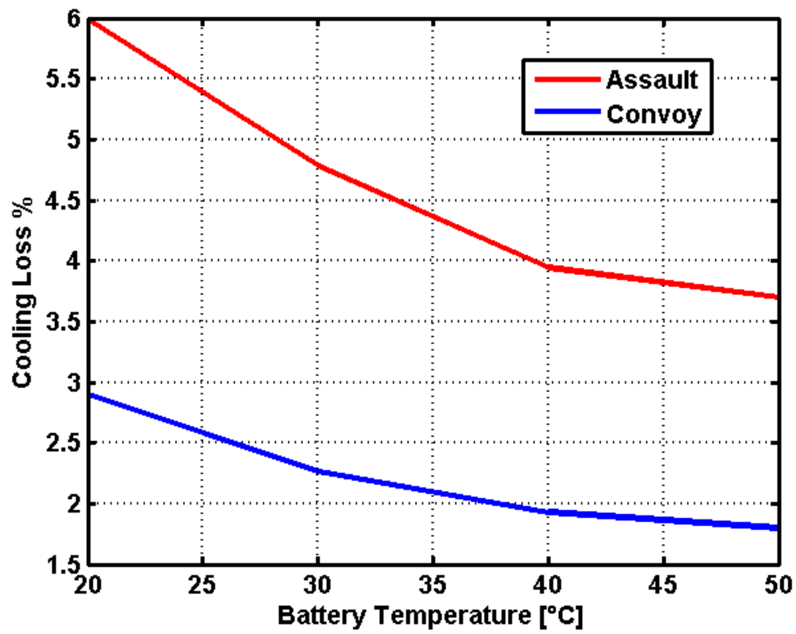

Figure 3.7: Fuel Economy Loss due to cooling requirement

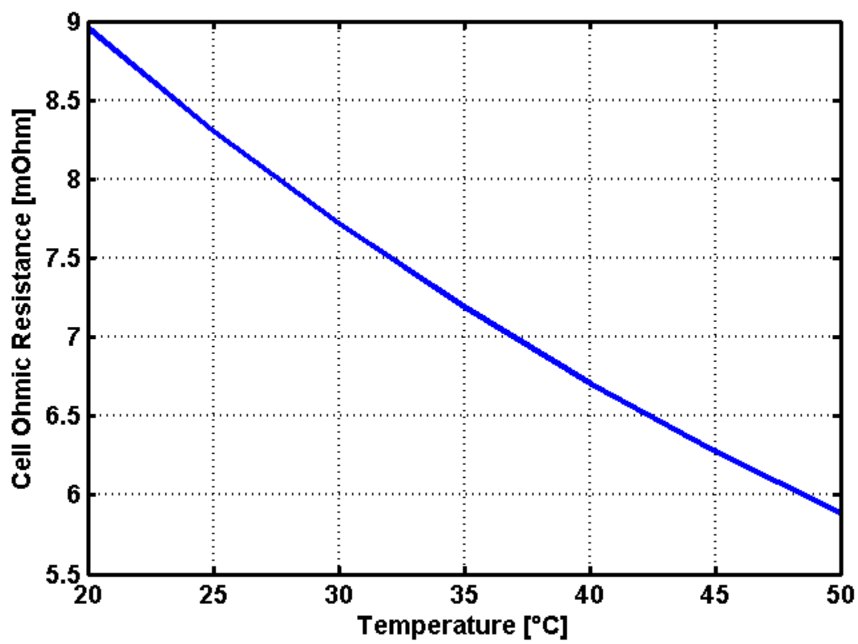

Figure 3.8: Ohmic Resistance of battery cell as a function of battery temperature

3.3 Long-term simulation- consideration of battery side reaction

This section runs long-term simulation, and analyzes the impact of battery side reaction on fuel efficiency and battery lifetime. Battery temperature varies from 30°C to 50°C, and the simulation for each case terminates when battery capacity loss reaches to 30%. Figure 3.9 shows the MPG result as a function of simulation cycle numbers.

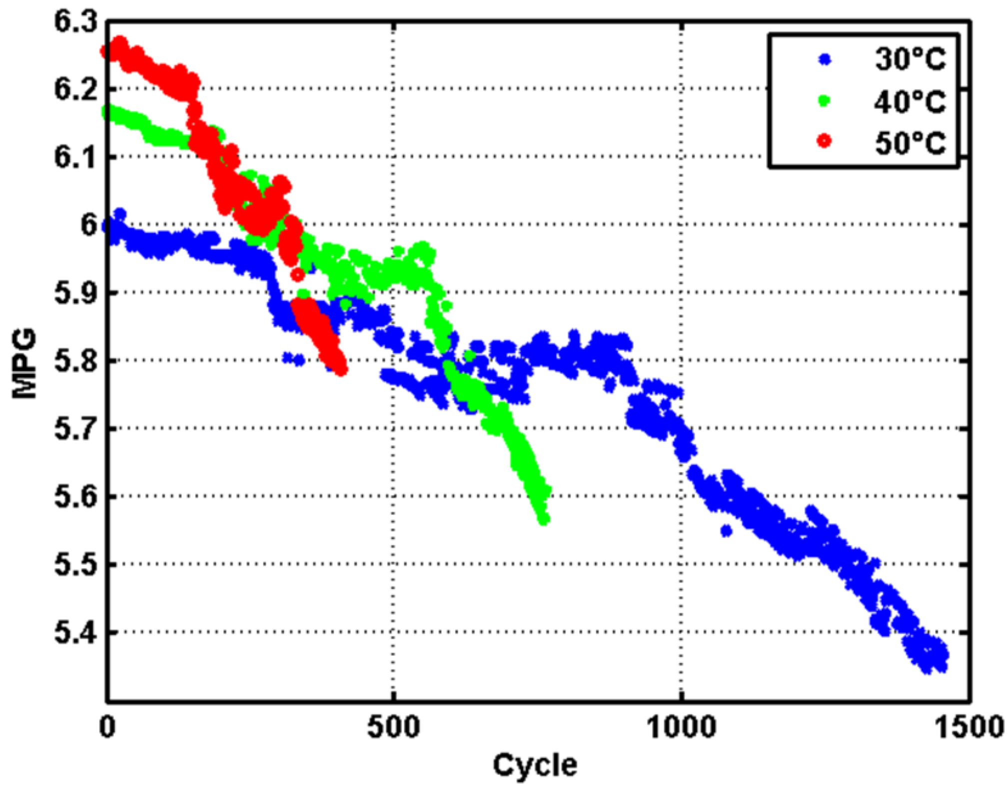

Figure 3.9: MPG under different battery temperature for long-term simulation

First, it was found that battery side reaction can lead to a significant MPG loss. For the case of battery temperature target of 40°C, the MPG drops by 9.6 % at the end of simulation. Both capacity fading and power fading have a tangible impact on vehicle efficiency.

The capacity fading is attributed to the irreversible consumption of lithium ions. As the capacity drops, the SOC varies quicker with time for the same current input. This causes more frequent battery charging and discharging, as shown in Figure 3.10, and hence more frequent use of cooling system. Battery power fading is related to the rise of ohmic resistance due to the resistivity of the growing SEI layer, and the reduction of the electrode effective transport properties. The increase of internal resistance leads to higher heat generation rate under the same current, as shown in Figure 3.11. Overall, the total generated heat per cycle increases by 29%, and most of that can be attributed to the impact of power fading.

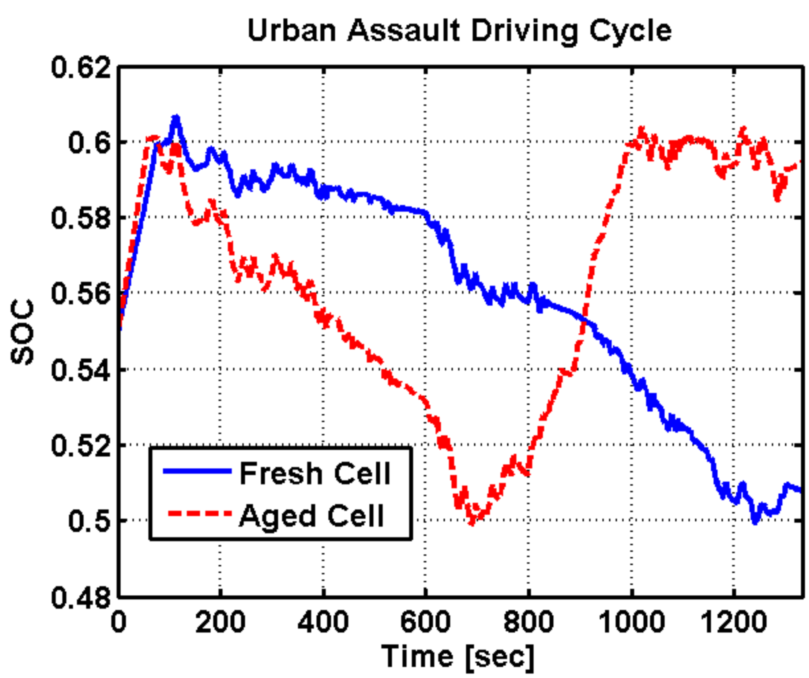

Figure 3.10: SOC trajectory with baseline control strategy. Battery temperature is targeted at 40°C.

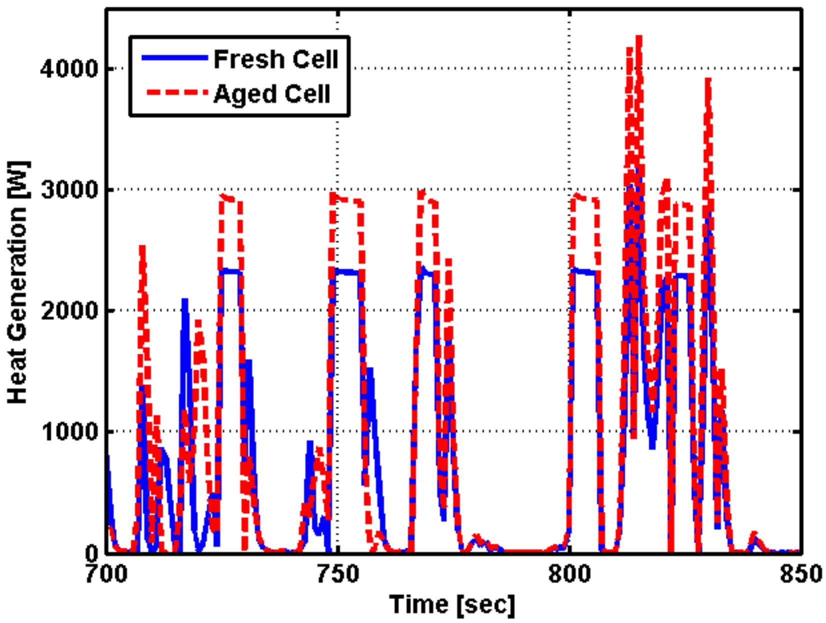

Figure 3.11: Heat generation of battery pack.

Second, battery target temperature impacts both lifetime and system efficiency. With fresh battery cells, high temperature could improve MPG. However, it accelerates aging rate, and hence the loss of MPG. Comparing with the case of 40 and 50°C, the MPG under 50°C drops below 40°C after 300 cycles.

3.4 Summary

This chapter studies the impact of battery cooling and side reaction of electrolyte decomposition on system performance.

The short-term result shows that battery thermal management has significant impact on fuel economy. When battery temperature is set as 40°C, the penalty due to the operation of the refrigerant-based battery cooling system in an S-HEV can be as high as 5% in case of urban assault driving cycles. Lower battery temperature target increases cooling loss. The long-term simulation shows that the side reaction not only reduces battery life. It also causes system efficiency loss of electrified powertrain. Due to the thermal effect on reaction rate, battery aging was accelerated at elevated temperature. It also accelerates fuel efficiency loss.

CHAPTER FOUR

OPTIMIZATION OF SUPERVISORY CONTROL FOR SERIES HEV WITH CONSIDERTION OF BATTERY SIDE REACTION AND COOLING LOSS

This chapter develops a methodology to optimize the supervisory controller for heavy-duty series hybrid electric vehicles with objectives of fuel economy and battery aging. Power management and battery thermal management are integrated in the optimization problem. Two objectives, namely fuel economy and battery life, are included by weighted sum method. Battery Aging model, thermal model, and cooling model are simplified in the optimization procedure with reduced state numbers. A sub-optimal but real-time implementable algorithm, stochastic dynamic programming, is applied to solve this problem. And the generated control strategy is embedded into the controller of high-fidelity model for simulation.

Several studies have been published that considers battery aging as additional objective. The Ah-throughout aging model combined with equivalent circuit battery model (Ebbessen et al., 2011) (Serrao et al., 2011) (Ebbessen et al., 2012) (Li et al., 2014) (Suri et al., 2016) has been studied for plug-in or parallel HEVs, with considering c-rate or SOC. In these studies, the rate of capacity fading is quantized by equivalent Ah throughout. The electrochemical based model for solid electrolyte interphase (SEI) growth was first used by Moura et al. (Moura et al., 2013) for plug-in HEV. In the power management optimization, the electrochemical based aging model is simplified into a static map, and the SEI growth rate is represented as a function of current and state of charge. In previous work, the thermal effect on aging rate was considered by Sciarretta

(Sciarretta el al., 2014) and Suri et al. (Suri et al., 2016), but the cooling power consumption was neglected.

Stochastic dynamic programming (SDP) approach has been proposed in supervisory control problem. Lin et al. (Lin et al., 2003 and 2004), and Jahannesson et al. (Jahannesson et al., 2007) proposed SDP strategy for the supervisory control of parallel HEV. Moura et al. (Moura et al., 2011 and 2013) applied SDP strategy for plug-in HEV. Johri el al. (Johri el al., 2009) applied SDP strategy for series hybrid hydraulic vehicle, with additional objective of determining the best operating regime for fulfilling the optimized power demand. Most studies considered fuel economy as single objective. Lin el al. (Lin el al., 2004) considered emissions as additional objective, and Moura et al. (Moura et al., 2013) considered battery life as additional objective.

In this chapter, we propose a SDP approach for the supervisory control of series HEV. A static map based on electrochemical-based aging model is used, and the thermal effect on aging rate is included. Power management and battery thermal management are integrated, and the cooling consumption from compressor is considered in addition to vehicle propulsion. This chapter is organized as follows. The first section describes problem formulation. The second section describes the optimization procedure. The third section compares SDP strategy with baseline strategy for short-term and long-term simulation. Next the tradeoff between fuel economy and battery life is studied by sweeping the weighting factor in objective function. This chapter ends with summary.

4.1 Problem Formulation

The purpose for the optimization of supervisory control is to get a stationary control policy that chooses actions based only on the present state, without knowledge of future driving mission. Hence we formulate this problem as a constraint infinite horizon problem with stochastic data, defined as Eq.

Minimize:

$$\mathrm{E}\sum_{t=0}^{\infty}\lambda^{t} g(\mathrm{x}_t,\mathrm{u}_t,\mathrm{W}_t) \tag{4.1}$$

Subject to:

$$x_{t+1} = f(x_t,u_t,W_t) \tag{4.2}$$

$$x \in X \tag{4.3}$$

$$u \in U \tag{4.4}$$

where t is time, x_t is the state vector, u_t is the control vector, and W_t is the disturbance vector. g is the instantaneous cost function. f is the system model.

The objective function is to minimize the expected total cost over an infinite horizon. λ is the discount factor between 0 and 1. It implies the present cost is more important than the cost in the future, and guarantees the convergence of objective function.

The instantaneous function g is defined in Eq.4.5. It constructs a single objective by the weighted sum of two objectives, namely fuel consumption rate and active lithium ion consumption rate. The fuel consumption rate is computed by the combined BSFC map in Figure 3.2. The input, engine power, is one of control action. The active lithium ion consumption rate is related with side reaction rate i_s. The model of side reaction rate is simplified in optimization procedure, and the simplification is described in next section. In order to avoid scaling issue in computation, the objectives are normalized and take value from 0 to 1. The relative weight, *w*, determines the contribution of fuel consumption rate to the total cost, and its value varies between 0 and 1.

$$g(x_k,u_k,w_k)=w\frac{\dot{m}_{fuel}-\dot{m}_{fuel,min}}{\dot{m}_{fuel,max}-\dot{m}_{fuel,min}}+(1\text{-}w)\frac{\dot{Q}_s-\dot{Q}_{s,min}}{\dot{Q}_{s,max}-\dot{Q}_{s,min}} \tag{4.5}$$

The optimization of supervisory control is a constrained problem that needs to satisfy the limit for both states and control inputs. The constraints are defined as:

$$\begin{aligned}
&0 \le P_{eng} \le P_{eng,\max} \\
&0 \le P_{eng} \le P_{eng,\max} \\
&P_{bat,\text{charge}} \le P_{bat} \le P_{\text{bat,discharge}} \\
&0 \le P_{compressor} \le P_{\text{compressor,max}} \\
&SOC_{\min} \le SOC \le SOC_{\max} \\
&T_{bat,\min} \le Tbat \le T_{bat,\max}
\end{aligned} \tag{4.6}$$

These constraints correspond to component safety operation, and are considered into the instantaneous cost function by penalty method.

The disturbance W_t comes from the driver's command, and is modeled as a discrete Markov process. The probability distribution of power demand at next step is counted using the naturalistic driving cycles based on randomly selected drivers. Figure 4.1 shows the transition probability matrix for wheel speed of 54 rad/s. It is used to generate the next power demand based on current vehicle power and speed.

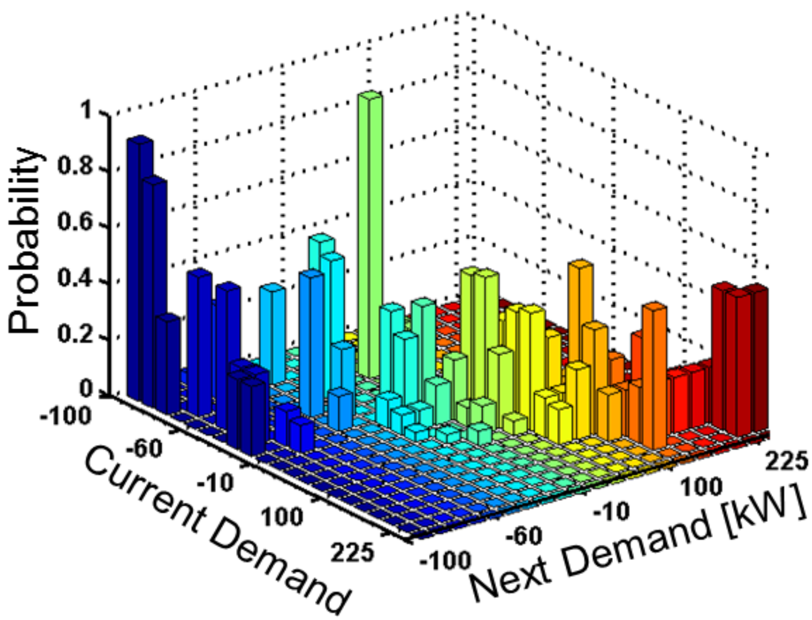

Figure 4.1 Transition probability matrix of power demand (wheel speed 54 rad/s)

4.2 Model Simplification

To consider additional objective of battery life, the prediction of battery aging rate, which is governed by the reaction rate of electrolyte decomposition, is needed in objective function. The electrochemistry-based model used in simulation framework achieves the required accuracy, but it is computational expensive. Hence, the number of states is reduced by choosing the N value in Eq. 2.31 as zero; the spatial effects of diffusion is removed, and the surface Li^+ concentration is represented by the average Li^+ concentration. Figure 4.2 shows the reaction rate of electrolyte decomposition (i_s) related with C-rate, battery temperature, and normalized average Li^+ concentration.

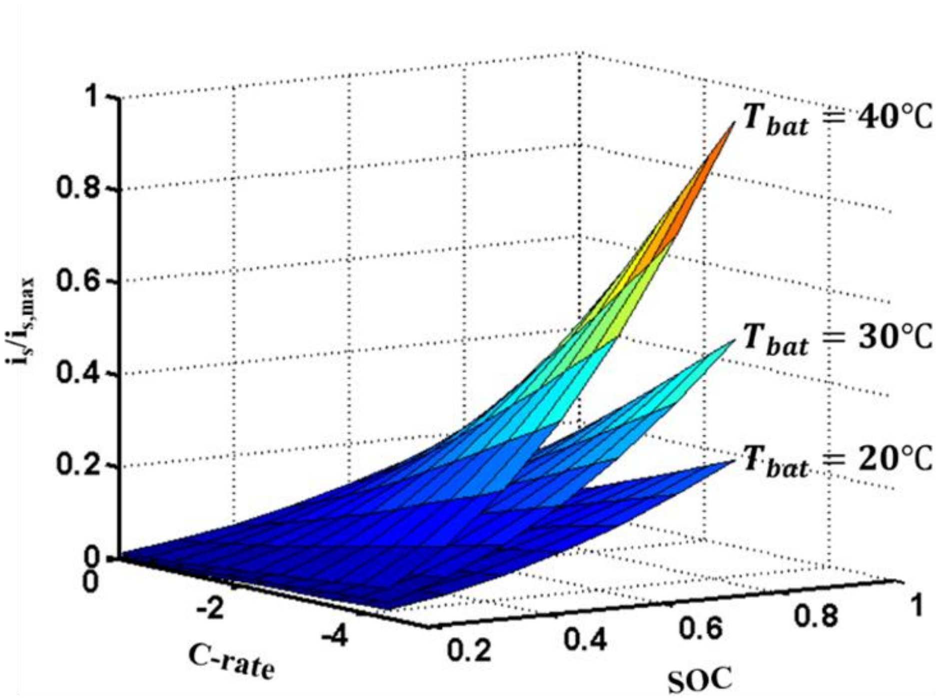

Figure 2.2: Normalized reaction rate associated with electrolyte decomposition as a function of current, SOC, and battery temperature.

The battery electrical model is simplified into an ideal open-circuit voltage source V_{oc} and an internal resistance R_{ohm}. The value of C-rate is calculated as:

$$I_b = \frac{V_{oc} - \sqrt{V_{oc}^2 - 4R_{ohm}P_b}}{2R_{ohm}} \tag{4.7}$$

$$C - rate = \frac{I_b}{C_0} \tag{4.8}$$

where P_b is battery power with positive value under discharging, and negative under charging, and C_0 is the ampere-hour (Ah) capacity.

The target of refrigerant-based cooling system is to sustain the core temperature of battery cells by actively varying cooling air temperature. In the simplified thermal model, cell core temperature is set as constant parameter, and the surface temperature varies in direct relationship with cooling air. The average temperature of battery core and surface is used as the input for determining battery aging rate. The cooling air temperature change is modeled based on the difference of heat generation and heat rejection, given as:

$$\frac{d}{dt}T_{air} = \frac{\dot{Q} - \dot{Q}'}{h_f} \tag{4.9}$$

where $\dot{Q}'$ is the heat removed from cooling air by the evaporator in the cooling system, and h_f is the convective heat transfer coefficient for cooling air. The heat generation rate ($\dot{Q}$) is calculated as:

$$\dot{Q} = I_b{}^2 R_{ohm} \tag{4.10}$$

The other components are modeled using efficiency maps, i.e. engine, generator, e-motors and cooling system. The driver's command is modeled as stochastic dynamic process by Markov chain; based on current vehicle speed and power demand, the power demand at the next step is generated using a transition probability matrix. After model simplification, the powertrain is modeled as a four-state system with two control variables. The states include vehicle speed, power demand, battery state of charge, and cooling air temperature. The control inputs are battery power and condenser power.

4.3 Optimization of Supervisory Control

4.3.1 Stochastic Dynamic Programming

Policy iteration algorithm searches for the optimal policy. It alternates between a policy evaluation and a policy improvement step and guarantees fast convergence on the optimal policy (Bertsekas et al., 2005). In policy evaluation step, given a policy π, the value function V_π is estimated by calculating the Bellman equation for each state, i.e.:

$$V_\pi^{n+1}(\mathrm{x}) = \mathrm{E}\{\mathrm{g}(\mathrm{x}, \pi(\mathrm{x}), \mathrm{w}) + \gamma V_\pi^{n}(\mathrm{x}')\} \tag{4.11}$$

This allows the subsequent policy improvement step; the Bellman is minimized to find the new policy π', with the estimated value function from last policy evaluation step.

$$\pi'(\mathrm{x}) = \arg\min_{u \in U} E\{\mathrm{g}(\mathrm{x}, \mathrm{u}, \mathrm{w}) + \gamma\, \mathrm{V}_\pi^{n+1}(\mathrm{x}')\} \tag{4.12}$$

This iterative process is repeated until convergence within a selected tolerance level. Finally a steady-state policy, which maps system states to control command, is generated in the form of a lookup table, and implemented into the supervisory controller of the high-fidelity S-HEV simulation.

However, due to battery aging, the parameters in system model (i.e., battery capacity and internal resistance) vary with time. The steady-state solution of SDP to the system with fresh battery cells is inappropriate to control the system with aged cells; the heat generation changes significantly, and consequently the optimal solution too. Hence, three steady-state policies are generated by SDP algorithm with different battery state of health, and the amount of lithium ion loss is used as a parameter to switch policies. Otherwise, the compressor energy would be underestimated, and the system would not be able to keep the battery temperature on target.

4.4 Improvements Achieved with SDP Optimization

This section discusses the improvements achieved by SDP strategy for both short-term and long-term simulation. The weighting factor in the cost function is set as one, which means only fuel economy is optimized as single objective. The resulting SDP strategies are implemented into the supervisory controller in the high-fidelity system model. Battery target temperature varies from 20°C to 50°C, the simulated driving cycles are Assault and Convoy cycle, and the ambient temperature is set as 49°C. Battery cells are assumed under fresh condition during short-term simulation, and the aging impact is only considered during long-term simulation.

4.4.1 Short-term Simulation with consideration of cooling loss

Table 4.1 lists short-term simulation result. Stochastic dynamic programming increases the overall fuel economy and reduced the penalty associated with parasitic cooling loss.

Table 4.1: Compare MPG and Cooling Loss of short-term simulation

<table>
<tr><td></td><td></td><td></td><td>20°C</td><td>30°C</td><td>40°C</td></tr>
<tr><td rowspan="5">Assault</td><td rowspan="3">MPG</td><td>ThermSOC</td><td>5.90</td><td>6.04</td><td>6.17</td></tr>
<tr><td>SDP</td><td>6.42</td><td>6.44</td><td>6.46</td></tr>
<tr><td>Improvement %</td><td>8.74</td><td>6.62</td><td>4.70</td></tr>
<tr><td rowspan="2">Cooling Loss %</td><td>ThermSOC</td><td>5.99</td><td>4.79</td><td>3.95</td></tr>
<tr><td>SDP</td><td>3.34</td><td>2.49</td><td>2.08</td></tr>
<tr><td rowspan="5">Convoy</td><td rowspan="3">MPG</td><td>ThermSOC</td><td>8.41</td><td>8.53</td><td>8.61</td></tr>
<tr><td>SDP</td><td>8.77</td><td>8.86</td><td>8.91</td></tr>
<tr><td>Improvement%</td><td>4.29</td><td>3.87</td><td>3.50</td></tr>
<tr><td rowspan="2">Cooling Loss%</td><td>ThermSOC</td><td>2.97</td><td>2.27</td><td>1.93</td></tr>
<tr><td>SDP</td><td>1.95</td><td>1.37</td><td>1.14</td></tr>
</table>

To gain knowledge from the SDP strategy about powertrain coordination, two situations are discussed in depth. The first is comparison of the SDP result obtained with and without cooling, in order to analyze how the cooling load changes the optimal decision. The second is the comparison of the dynamic programming strategy with the thermostatic SOC control, in order to analyze the benefit of integrating power and cooling system in a unified supervisory strategy, rather than considering them separately.

In SDP strategy without considering cooling load, cooling power is set as zero and battery is assumed to be in a thermal equilibrium status. In that case, the vehicle system is represented by a 1-state (SOC) system, with one control variable (power pack electric output power).

$$\alpha_{batt,dischg} = \frac{\int_0^N P_b \cdot (P_{veh} > 0) \cdot (P_b > 0) \cdot dt}{\int_0^N (P_{veh} + P_{cooling}) \cdot (P_{veh} > 0) \cdot dt} \tag{4.13}$$

When considering cooling loads/losses in SDP, battery discharge usage evaluated by Eq. 4.13 under propulsion is reduced by 3.99% so that the heat generation (cooling load) can be reduced too. This indicates the tradeoff between cooling loss and fuel consumption for battery discharging usage. Normally, more aggressive battery usage is beneficial for S-HEV fuel economy, but this analysis indicates that aggressive battery discharging leads to increased consumption by the cooling ancillary system. By tracking the cooling load for the whole cycle, the algorithm finds it beneficial to operate much more frequently in hybrid mode, rather than all-electric, thus leading to milder duty cycle for the battery. However, this will result in an increase in engine load, and this is something that will be examined in greater detail in the future. Battery regeneration during vehicle braking is reduced by 5.9% primarily by limiting the peak charging power. Related reduction of the cooling effort more than compensates for the small reduction of regeneration capacity.

Figure 4.3 compares the cooling power control sequence of SDP and baseline strategy. SDP operates the cooling system with high load during braking. Thus, 47% cooling power is provided by regeneration, and this maximizes utilization of braking power.

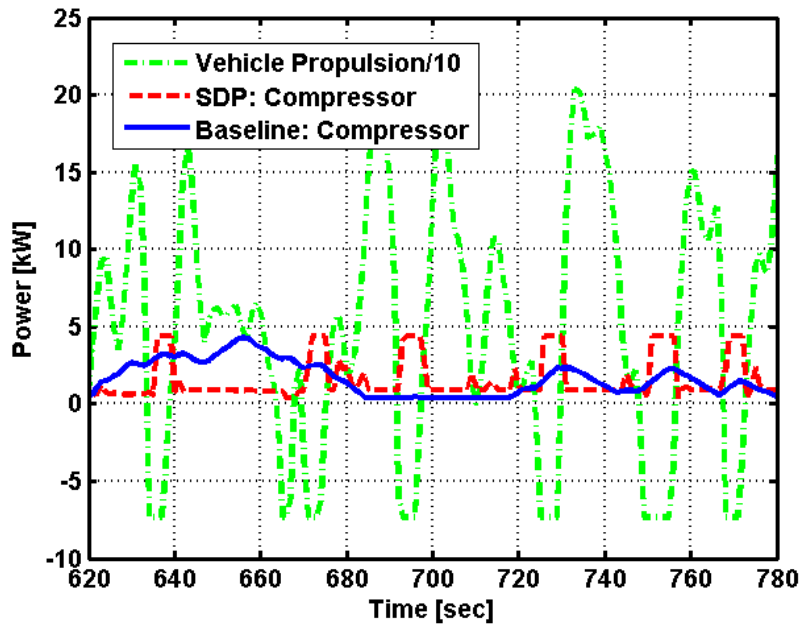

Figure 4.3: Comparison of Compressor command sequence. The red line is SDP strategy, and the blue line is the baseline strategy.

4.4.2 Long-term Simulation considering battery aging

This part compares long-term simulation result of SDP with baseline strategy. The target for battery core temperature is set as 40°C, and the driving cycle is urban assault cycle. The simulation ends when battery capacity drops by 30%. As shown in figure 4.4, SDP improves overall MPG and also prolong battery life.

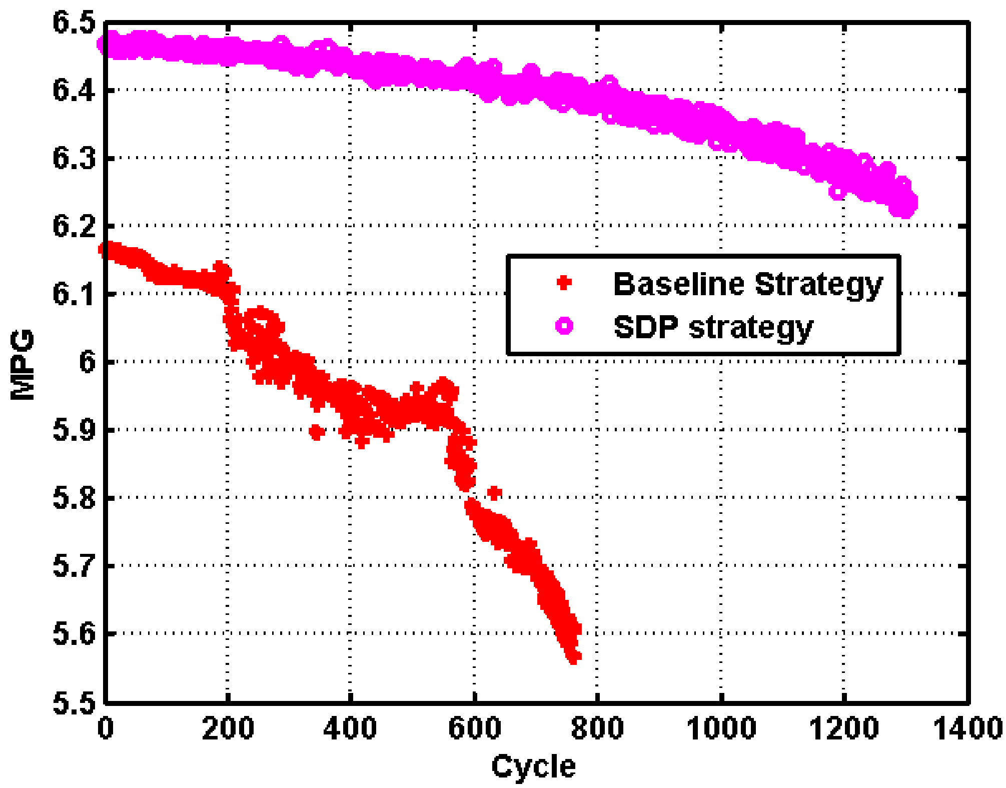

Figure 4.4: Compare long-term simulation result of SDP with Baseline strategy.

4.5 Tradeoff between fuel economy and loss of active lithium ions

This section investigates the tradeoff between fuel consumption and loss of active lithium ions. It focuses on analyzing how SDP strategy balances two conflicting objectives. The weighting factor in objective function sweeps from 0 to 1, and battery temperature target is set as 20°C, 30°C, and 40°C. The resulting SDP strategy is embedded into the supervisory controller of system simulation framework. The simulation runs for short term; the impact of side reaction on active lithium ions loss is considered, while its impact on long-term MPG loss is not included.

Figure 4.5 shows the tradeoff between normalized fuel consumption and lithium ions loss. When the weight w is zero, the battery is fully utilized to minimize the fuel consumption, and the lithium ions consumption is the highest. Comparing the condition of 30°C with 40°C of battery core temperature, fuel consumption is increased by 2.3% due to increased cooling requirement, but the loss of lithium ions is reduced by 47 %. As the weight increase from zero to one, fuel consumption increases while lithium ion reduces. Comparing with 30°C, the change of lithium ions loss is more sensitive to the change fuel consumption with battery core temperature of 40°C.

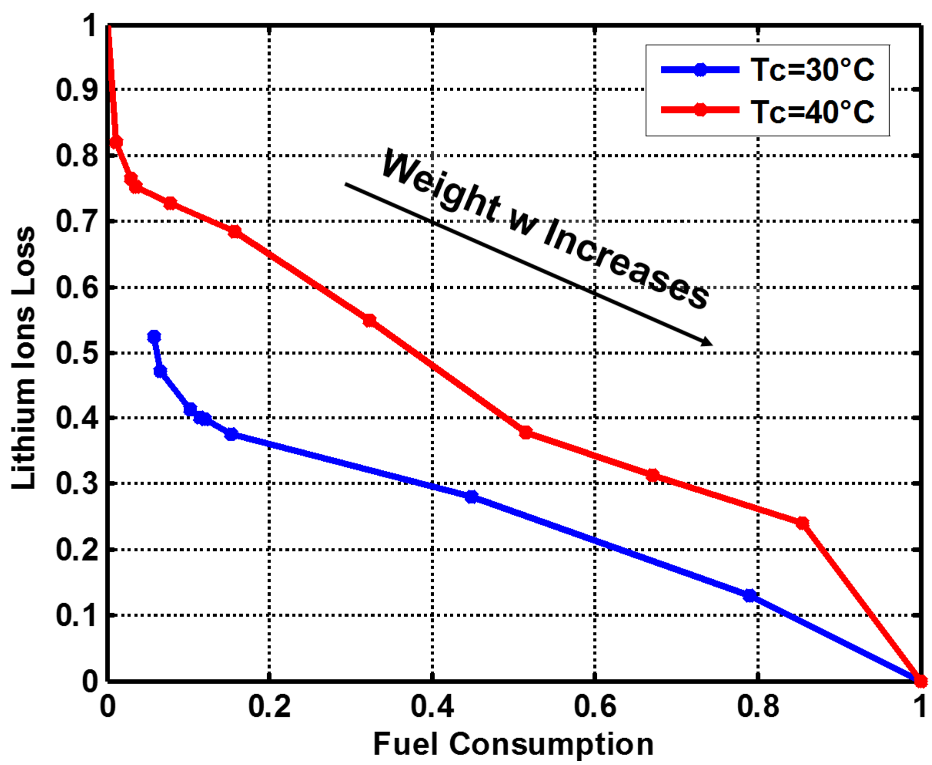

Figure 4.1: Tradeoff between fuel consumption and active lithium ion loss.

Figure 4.6 shows the battery command under different weighting factor under 40°C. The green dot line is vehicle power, and the positive value shows vehicle propulsion and negative shows vehicle regeneration. Overall as the weight for battery life increases, battery load cycle becomes milder to reduce the lithium losses. When the weighting factor is small and the fuel consumption governs the cost function, the maximum regeneration is maintained, and the engine-charging-battery event during vehicle propulsion is reduced comparing with w0 with w0.2. As the weight increases, battery regeneration starts to reduce. When the weight becomes one, the vehicle runs in traditional mode with only engine.

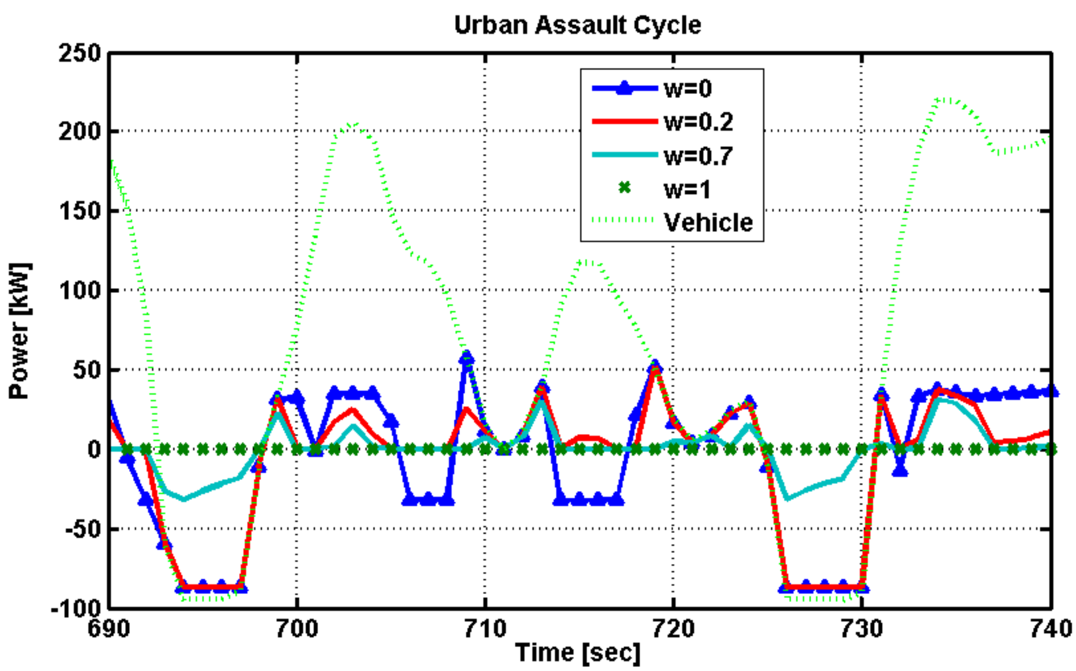

Figure 4.2: Comparison of the battery power sequences under Urban Assault Cycle, obtained for different weighting factors. Battery core temperature is set as 40 °C.

4.6 Summary

This chapter developed a real-time implementable supervisory control strategy for series HEVs based on stochastic dynamic programming. It considers the impact of battery cooling and side reaction in problem formulation, and a simplified average-SOC based battery aging model was proposed for the optimization procedure. Two objectives of fuel economy and battery life are optimized, and a set of strategies are generated with different weighting factors.

Compared to the baseline thermostatic strategy, SDP-generated controller improves both fuel economy and battery life under different battery temperature and driving cycles. Detailed analysis of results indicates a milder battery duty cycle, as well as the ability of the algorithm to maximize the usage of regeneration energy for operating the A/C compressor in the cooling system.

Tradeoff between fuel economy and battery life was analyzed. It shows the penalty of fuel economy to prolong battery life, and the amount of payment is impacted by battery temperature. Battery operation is modulated to balance two objectives under different weighting.

CHAPTER FIVE

OPTIMAL SUPERVISORY CONTROL OF SERIES HEV WITH CONSIDERATION OF LITHIUM ION DIFFUSION EFFECTS ON BATTERY FADING

This chapter expands the methodology to optimize the supervisory controller of series hybrid electric vehicle with multiple objectives, considering battery thermal management and a more accurate model of aging process. The fidelity battery aging model is enhanced by considering the dynamic impact caused by the effect of lithium ion diffusion; the number of Q_n in the approximate analytical solution of lithium diffusion is selected as 1. SDP algorithm used in the previous chapter was able to handle four states and two control inputs. However, with an additional state, the computer memory requirement and computation effort exceeded the capacity of current available hardware. A novel approach, neuro dynamic programming, is proposed to solve this problem with increased number of states. It combines the idea of functional generalization and temporal difference learning with dynamic programming, and holds a promise that the computation load increases linearly with the number of parameters in approximated function rather than exponentially with the number of states.

This chapter is organized as follows. The first section describes the optimization algorithm, neuro dynamic programming (NDP). The second section shows the validation and convergence of NDP using average SOC aging model; its result compares with SDP. The third section shows the improvement of NDP with surface-SOC aging model. This chapter ends with summary.

5.1 Neuro Dynamic Programming

Traditional application of the Dynamic Programming algorithm suffers from the curse of dimensionality. The state space is discretized into grid nodes, and the cost-to-go function need to be calculated for all nodes. The computational load increases exponentially with state space. Hence a new approach, neuro dynamic programming is proposed in this chapter, which combines the idea of reinforcement learning and dynamic programming. In neural dynamic programming, instead of calculating the true cost-to-go function, the algorithm use approximate cost-to-go function. By sampling the states from state space, the approximation function learns from the interaction with system. This holds a promise that the computation load increase linearly with the number of parameters in approximation function.

The neuro dynamic programming algorithm contains two parts, namely prediction of future cost and select control action. The prediction of future cost is to learning the approximated value function by the samples collected when simulating the system model forward. The control action is selected by the policy created using the approximated value function.

5.1.1 Approximating and Learning Value Function

Neural networks provide a powerful model to estimate nonlinear functions that have a large number of inputs. Let the approximation function represents as:

$$\tilde{J}(\mathrm{X}, r) = \sum r_i f_i\ (\mathrm{X}) \tag{5.1}$$

where f_i is the basis function that extract characteristics of state variables (X) on value function, and r_i is the parameters that need to learn.

Unlike supervised learning of neural network, there are not input-output sample pairs to update the parameters. Instead, the output we get from system simulation is the instantaneous cost, which is part of the value function. Hence, the parameters in approximate function are learned by the temporal difference (TD) learning method (Sutton et al., 1998).

Assume the present state is X_k, and the policy at present is π. Then the control input based on current state is:

$$u_k = \pi(\mathrm{X_k}) \tag{5.2}$$

By applying control action u_k to the system, an instantaneous cost $g(X_k, u_k, w_k)$ generated with next state X_{k+1}. And the predicted value of being in state X_{k+1} can be written as $\tilde{J}(X_{k+1}, r)$. Based on Bellman Equation (Bertsekas et al., 2011), the estimated value of being in state X_k can be written as:

$$J(\mathrm{X}_{k,}\, r) = g(\mathrm{X}_k, u_k, \mathrm{w}_k) + \tilde{J}\ (\mathrm{X}_{k+1,}\, r) \tag{5.3}$$

The problem to the optimal parameters for approximation is to reduce the error between estimated and predicted value function, defined as:

$$\begin{aligned} r \ &= \ \arg\min \frac{1}{2}(J(X_{k,}r) - \tilde{J}\ (X_{k,}r))^2 \\ &= \ \arg\min \frac{1}{2} d_k{}^2 \end{aligned} \tag{5.4}$$

with the temporal difference d_k defined as:

$$d_k = g(\mathrm{X}_k, u_k, \mathrm{w}_k) + \tilde{J}\ (\mathrm{X}_{k+1,}\, r) - \tilde{J}(\mathrm{X}_k, r) \tag{5.5}$$

Eq. 4.17 can be solved by iteratively updating the parameter by:

$$r_i := r_i + \gamma d_k \nabla_r J(\mathrm{X_k}, r_i) \tag{5.6}$$

The gradient $\nabla_r J(X_k, r_i)$ is calculated using Levenberg-Marquardt method, defined as:

$$\nabla_r J(\mathrm{X_k}, r_i) = -(J^T J + \mu I)^{-1} J^T \tag{5.7}$$

where J is the Jacobian matrix.

5.1.2 Policy Update

The policy function is represented by a separate neural network, represented as:

$$\pi\left(\mathrm{X}, \theta\right) = \sum \theta_i \phi_i \ (\mathrm{X}) \tag{5.8}$$

This study used greedy policy based on approximated value function. The control action could be written as:

$$u_\mathrm{k} = \mathrm{argmin}(g(\mathrm{X}_k, u_k, \mathrm{w}_k) + \tilde{J} \ (\mathrm{X}_{k+1,} \ r)) \tag{5.9}$$

And the parameter set in policy π approximation can be updated by supervisory learning method with state-action pairs (x_k,u_k).

5.1.3 Learning and Control

Previous two sections described learning of value function and policy function, respectively. This section builds the process of updating policy while learning the approximate value function simultaneously, using the approximate policy iteration method (Powell et al., 2011). It can be viewed as actor-critic control. The policy is known as actor that selects a control command given the state. The environment is the system. The system runs the control command and generates next state and the instantaneous cost. Then the TD error is used to update the critic, and then the control policy is updated by minimizing the Bellman equation based on the updated critic. Figure 5.1 shows the pseudocode of NDP algorithm with approximate policy iteration.

To avoid implementing infeasible actions during learning process, the feasible region of control actions is calculated beforehand and saved into the system model. When the control action selected using current learned policy is out of feasible region, then any feasible action is implemented instead.

1. Input:
   - Neural Network structure for value function
   - Neural Network structure for policy function
2. Initialization:
   - Value function parameters
   - Policy parameters
   - Initial state x_0
3. For k=0,1,2,… do
   - Measure x_k
   - Select action $u_k = \pi(x_k|\theta_k)$
     - If not feasible, select u_k from feasible set
   - Execute u_k
   - Observe x_{k+1}, $\mathrm{g}(x_k, u_k, W_k)$
   - TD error: $d_k = \mathrm{g}(x_k, u_k, W_k) + \tilde{J}(x_{k+1}, r_k) - \tilde{J}(x_k, r_k)$
   - Critic Update: $r_{k+1} = r_k + \gamma d_k \nabla_r J$
   - Actor Update: $u_k' = argmin(\mathrm{g}(x_k, u_k, W_k) + \tilde{J}(x_{k+1}, r_{k+1}))$

     $$\theta_{k+1} = \theta_k + \gamma(u_k' - u_k)\,\nabla_\theta \pi$$
4. Endfor
5. Return function parameters

Figure 5.1: Pseudocode of NDP algorithm with approximate policy iteration

5.2 Improvement of Computation Efficiency with NDP algorithm

This section shows the improvement of computation efficiency by NDP algorithm. The result compares with SDP algorithm using two simplified system models, namely (i) basic powertrain model with 1 state (*SOC*) and 1 action (P_{gen}), and (ii) powertrain model considering cooling system with 2 states (*SOC*, T_{air}) and 2 actions (P_{gen}, $P_{cooling}$). In the problem formulation, battery temperature is set as 40°C, and fuel economy is considered as single objective. Assault and Convoy cycles are simulated for short term. The NDP learning process stops when the approximate cost-to-go function converge, as shown in Figure 5.2, and the policy update process with cost-to-go function learning is illustrated in Figure 5.3.

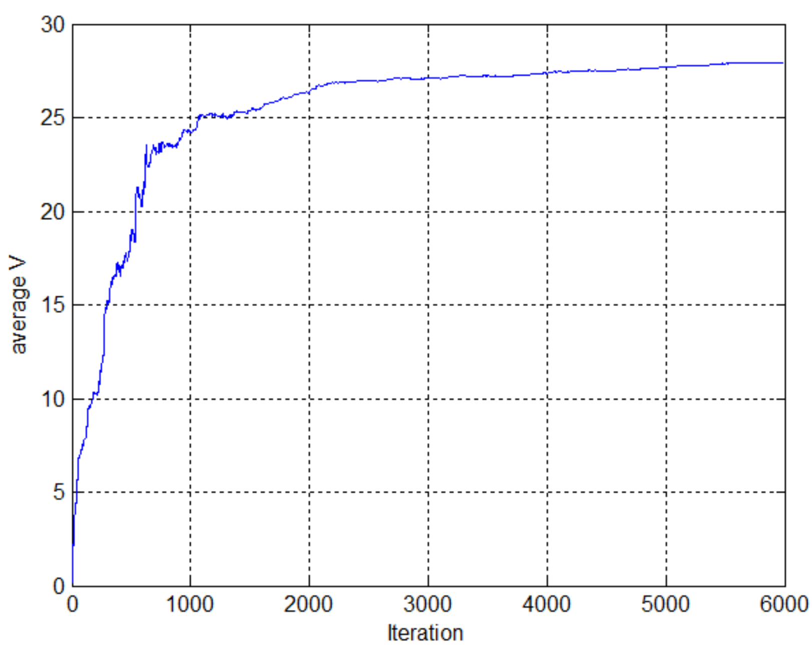

Figure 5.3: Iteratively Learning of Approximate Value function

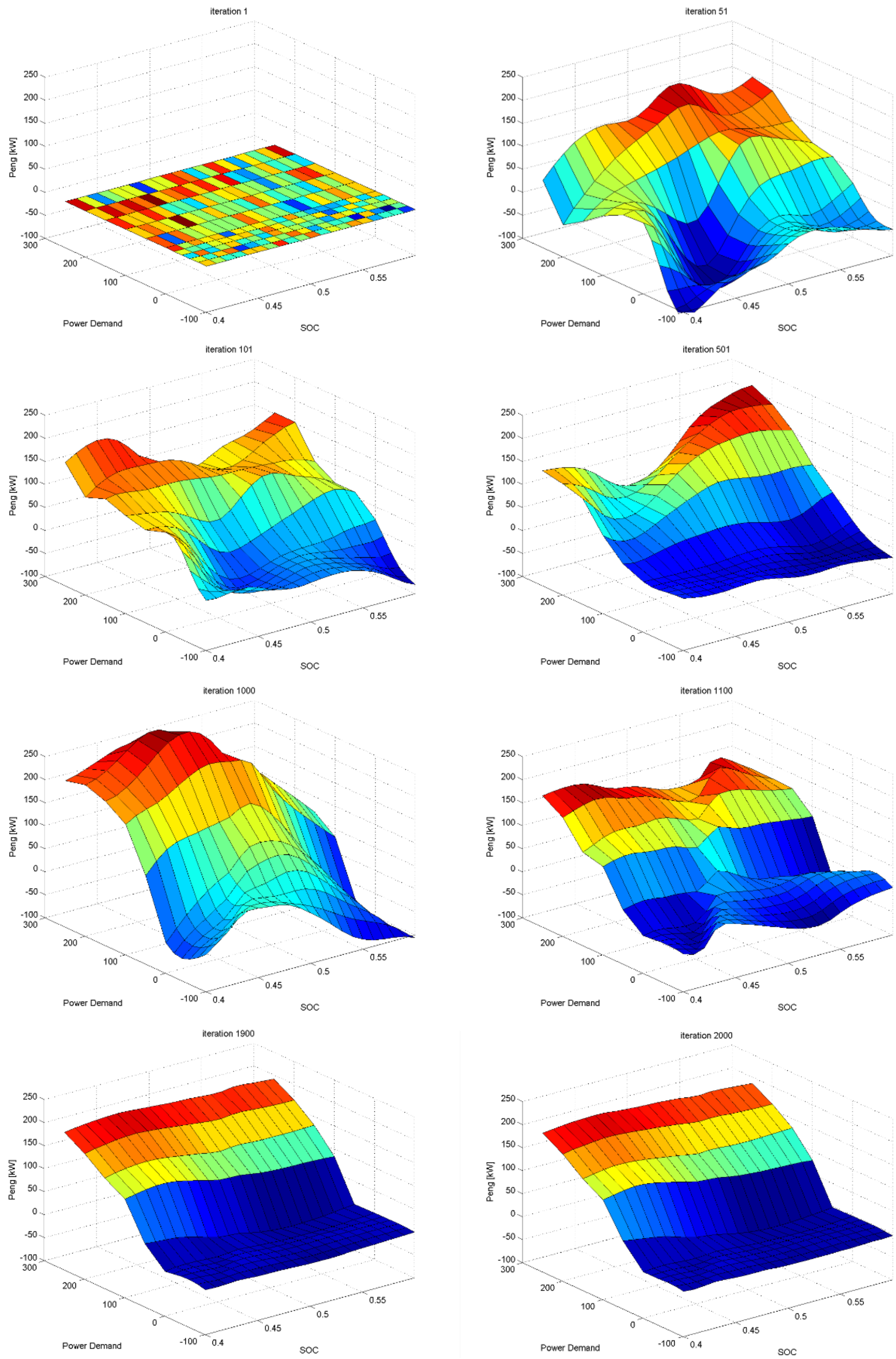
iteration 1
iteration 51
iteration 101
iteration 501
iteration 1000
iteration 1100
iteration 1900
iteration 2000
Peng [kW]
Power Demand
SOC

Figure 5.3: Policy Update sequence with the value function learning process. Initial steps produce few infeasible points, but convergence eventually yields a smooth surface

The difference between SDP and NDP strategy is quantized by:

$$\max\left\| P_{eng}^{NDP} - P_{eng}^{SDP} \right\| \tag{5.10}$$

And the maximum value is estimated using a sample set that is uniformly distributed in state space. The maximum difference is less than 1 kW.

Figure 5.4 and 5.5 shows the operation point on combined-BSFC map with SDP controller and NDP controller, respectively. The color scale reveals the frequency of the operation point. It can be seen similar engine operations. This indicates that NDP with neural network approximation could find the policy that is close to SDP optimization.

The second observation from maps is that the optimal strategy does not always operate engine in the sweet spot. System efficiency effects clearly override the component-centric reasoning. The engine often operates at modest power levels during hybrid operation enables by high battery SOC, but remains close to the best-BSFC line, as indicated by the yellow/red spot below 1000 RPM. In this case, relatively small compromise on engine efficiency is more than compensated for by the effective use of regenerated energy. Figure 5.6 shows the power sequence of engine and vehicle. It can been seen that engine load cycle is milder with assistance of power source from battery, comparing with conventional vehicle in which vehicle power is provided all by engine.

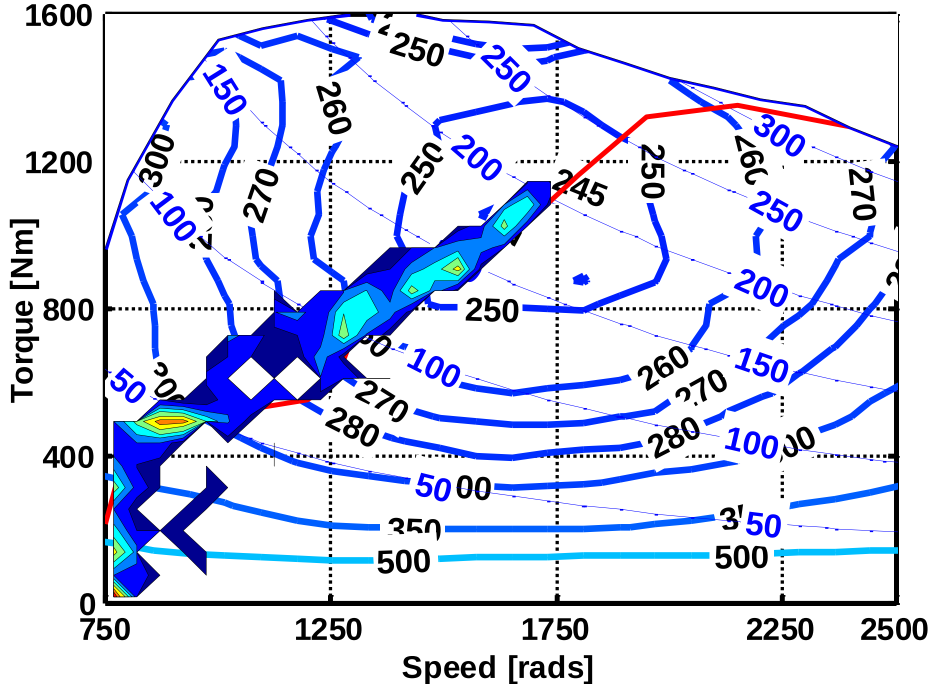

Figure5.4: Engine Operation Point on Combined BSFC map with SDP strategy

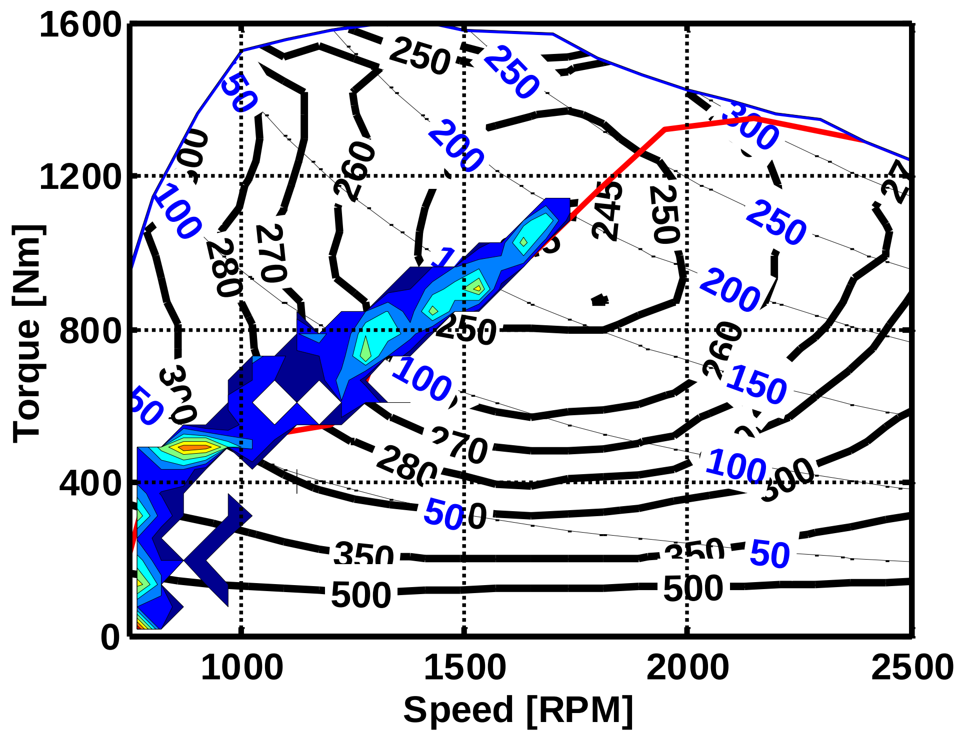

Figure5.5: Engine Operation Point on Combined BSFC map with NDP strategy

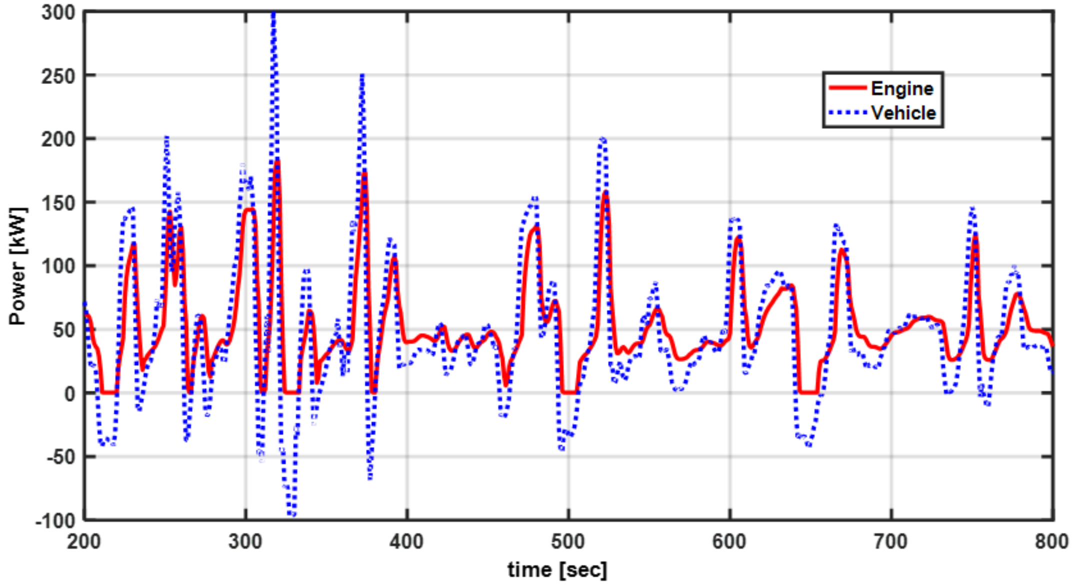

Figure 5.6: The power sequence of engine and vehicle with SDP control strategy under Convoy Cycle

As shown in Table 5.1, NDP algorithm could reduce the computational time comparing with SDP algorithm. As the state number increases, the improvement becomes large. This provides a promising algorithm to extend the system model to a large state-action space with handling complex problems.

Table 5.1: Compare result of NDP with SDP

System Model	Algorithm	Computation [hour]
4 variables	SDP	0.8
	NDP	0.5
6 variables	SDP	10
	NDP	3.8

5.3 Improvement of fuel economy and battery life with Surface-SOC based battery aging model

In this section, surface-SOC based battery aging model is used in NDP optimization. The state variables X include battery state of charge (SOC), cooling air temperature (T_{air}), SEI thickness (δ_{SEI}), and Li^+ surface concentration ($\boldsymbol{c_s}$) which represents by the average concentration ($\bar{c}$) and a series of eigenfunction (Q_n). The control inputs u include the output electric power of power pack (P_{gen}) and cooling power ($P_{cooling}$).

The number of eigenfunction is selected as 1, and the normalized Li^+ surface concentration is written as:

$$C_s(\tau) = \overline{C}(\tau) + Q_1(\tau) + err_n(\tau) \tag{5.11}$$

As shown in figure 5.6, even though the approximate surface concentration with one eigenfunction (Q_1) still shows an error in predictions compared to FDM solution, it is able to capture the instantaneous dynamics and far superior to using the average concentration. The approximate solution reduces the error of active lithium ion loss per driving cycle from 11% to 4% compared with the average concentration.

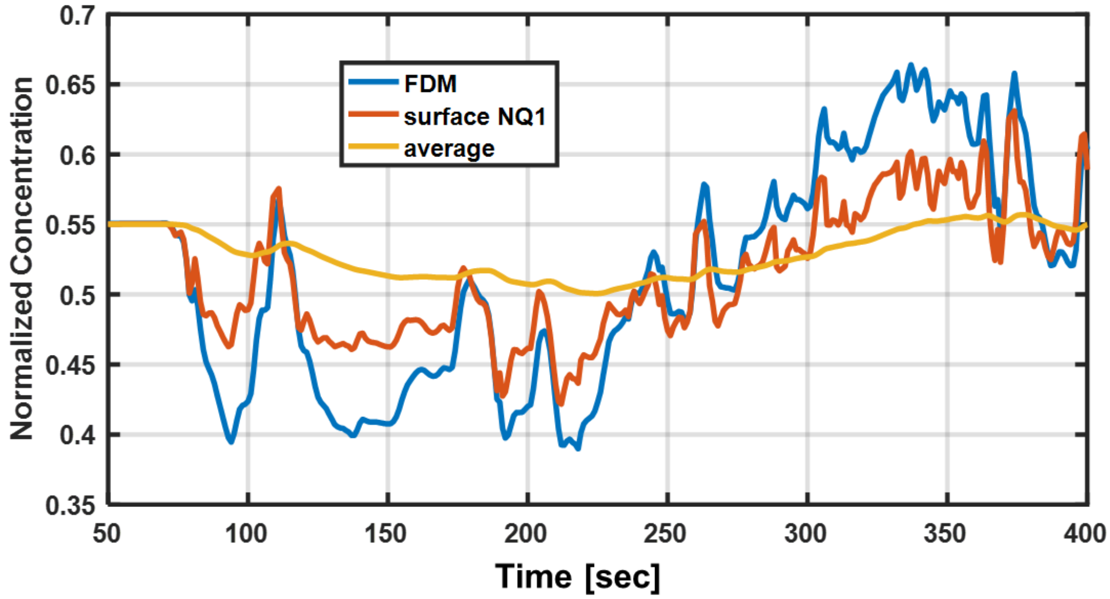

Figure 5.7: Compare Lithium concentration of surface concentration, average concentration, and approximate surface concentration (NQ=1)

In order to keep the instantaneous Li^+ surface concentration within reasonable range, limitations are set on each term in eq. 82. The penalty term for surface concentration is added into the instantaneous cost function as:

$$g(x_k, u_k, w_k) = w\frac{\dot{m}_{fuel} - \dot{m}_{fuel,min}}{\dot{m}_{fuel,max} - \dot{m}_{fuel,min}} + (1-w)\frac{\dot{Q}_s - \dot{Q}_{s,min}}{\dot{Q}_{s,max} - \dot{Q}_{s,min}} + \beta(C_s - C_{s,min})^2 (C_s < C_{s,min}) \tag{5.12}$$

where β is the penalty factor.

This avoids the algorithm to generate infeasible solutions for surface concentration. As shown in Figure 5.8, without penalty, the surface concentration continues to decrease over time as the algorithm learns how to reduce side reaction rate. The concentration even goes to negative value. When the penalty term is added, the surface concentration drops at the beginning. After iteration 800, the algorithm receives high penalty cost, and increases the concentration to reduce the penalty. By adding the penalty term, the algorithm is able to keep surface concentration above reasonable value.

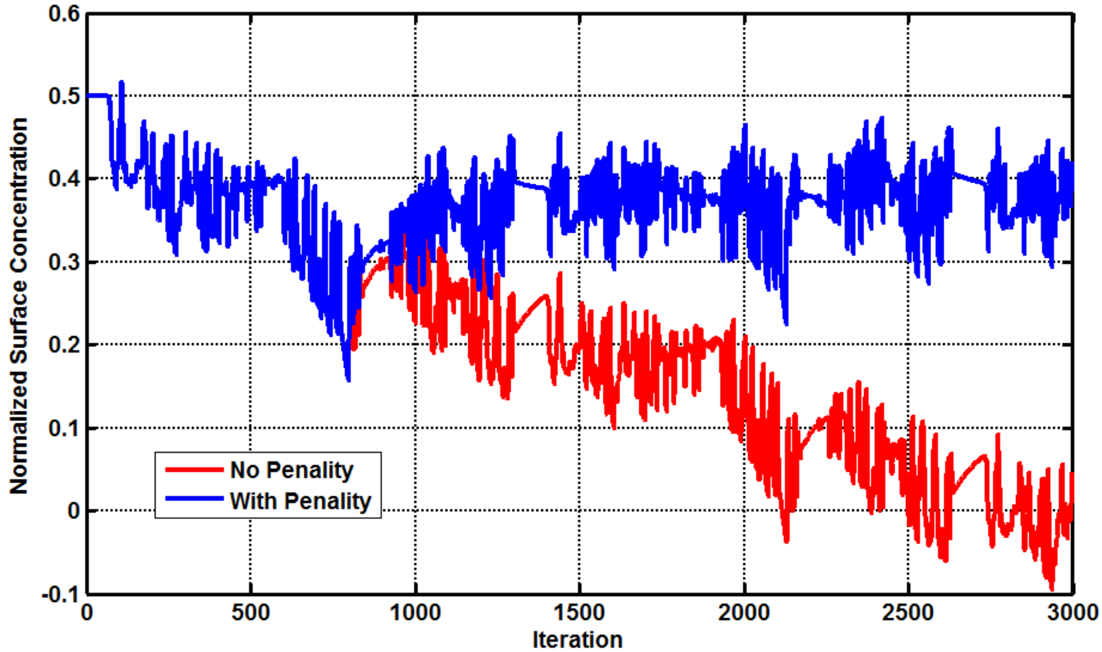

Figure 5.8: Trajectory of surface Li^+ concentration with NDP strategy with or without penalty

Table 5.2 shows the improvement of MPG and lithium ion loss from short-term simulation. The result is compared with SDP result in last chapter, which uses average-SOC based battery aging model in optimization. Battery temperature is set as 40 degC, and simulated cycle is Assault Cycle. The weighting factor is set as 0.25 for both SDP and NDP. It can be seen that comparing with SDP strategy, NDP strategy improves the lithium ion loss by 3.8% per driving cycle without penalty on fuel economy.

Table 5.2: Compare result of NDP with SDP strategy

	MPG	**Lithium Ion Loss**
SDP	6.35	0.52
NDP	6.39 (+0.6%)	0.50 (-3.8 %)

5.4 Summary

This chapter develops a framework for optimizing the supervisory control of series HEV system. The prediction accuracy of battery aging model under aggressive dynamic load cycles is improved by considering the diffusion delay of lithium ions. It increases the number of states and brings challenges to optimization algorithm. A computational efficiency algorithm, neuro dynamic programming, is proposed. With complex model and advance algorithm, both fuel economy and battery life are improved.

CHAPTER SIX

CONCLUSIONS

6.1 Summary

This dissertation develops a framework for optimizing the supervisory control for series hybrid electric vehicles with multiple objectives. In particular, we considered the impact of battery cooling and side reaction in system-level study to optimize the control for both fuel consumption and battery life.

Chapter two describes a unified series HEV simulation framework with models of key components and subsystems. A refrigeration-based cooling model is integrated, the compressor and air fans consume additional power, and it is considered in addition to vehicle propulsion power. To address battery life as additional objective, an electrochemistry-based aging model of Graphite-LiFePO4 battery is integrated, and the aging mechanism considered is the growth of solid electrolyte interphase (SEI) film. The impact factors include current, lithium ion concentration at electrode surface, and battery temperature. Model enables capturing the effect of capacity fading and power fading on system performance. This fully integrated S-HEV propulsion system model simulation provides a tool for systematic screening of the supervisory control strategy for two objectives, fuel economy and battery life.

In chapter three we analyze the impact of battery cooling and side reaction associated with SEI growth on system performance. A rule-based control strategy, thermostatic SOC control, is embedded into the power management module to control the power distribution between the power pack and battery pack and establishes a baseline. A model predictive controller is embedded into the thermal management module to control the cooling system. The result shows both battery cooling and side reaction to impose significant penalty on fuel economy. Elevated battery temperature could reduce the penalty from auxiliary cooling consumption. However, it reduces battery aging, and accelerates fuel economy loss associated with side reaction.

In chapter four, stochastic dynamic programming is applied to optimize the supervisory control strategy. It integrates power management and battery thermal management, and optimizes two objectives, namely fuel economy and battery life. Due to the ‘curse of dimension’ issue of classical dynamic programming, a simplified battery aging model is used in the optimization algorithm by ignoring the diffusion dynamics in the aging model; the lithium ions concentration on the electrode surface is replaced by the average concentration inside of electrode. The number of states is limited to four, with two control inputs. Improvement on both fuel economy and battery life compared to a Thermostatic SOC control is significant. Further, the tradeoff between fuel consumption and active lithium ions loss is studied by varying the weighting factor. Reducing active lithium ions loss penalizes fuel economy, and is impacted by battery temperature.

Finally, we include higher accuracy battery model in optimization framework, and propose neural dynamic programming algorithm. Improvement stews from consideration of surface lithium ions concentration. However, the number of states increase to the point of making the application of SDP unfeasible. Rather, a novel approach based on neuro-dynamic programming algorithm is pursued, which combines the idea of functional approximation and temporal learning with dynamic programming. With the enhanced battery model, the NDP algorithm successfully finds a strategy which further improves fuel economy and battery aging.

6.2 Main Contributions

This dissertation develops a framework to design a supervisory controller for series hybrid electric vehicle through multi-variable, multi-objective optimization of the vehicle power system. The main contributions can be summarized as:

- Developed a multi-physics, high-fidelity, and yet computational-efficient simulation tool for in-depth studies of series HEV system for a heavy vehicle
    1. Integrated an electrochemical aging model for Lithium-ion battery with the thermal effect, a lumped-parameter thermal submodel, and refrigerant-based cooling model into the S-HEV powertrain system simulation.
    2. Analyzed the impact of battery capacity fading and power fading on fuel efficiency and battery life, with consideration of cooling system parasitic losses
- Developed a framework to optimize the supervisory control of the vehicle power system considering both fuel efficiency and battery life. Emphasized ability of the algorithm to handle a large state-action space.
    1. Investigated the potential of Stochastic Dynamic Programming (SDP) to handle a problem with a combined fuel efficiency/battery life objective. Created a framework that leverages a battery electro-chemical single-particle model with approximate solution, i.e. a model capable of predicting SEI from

C-rate and average SOC. State-action space was characterized by four states and two control inputs. Shown that SDP is able to generate real-time implementable control strategies, and investigated the tradeoff between fuel economy and battery life, with consideration of battery thermal management.

2. Enhanced the predictiveness of the battery single-particle model by considering dynamic load cycles and their impact on the Li-ion surface concentration. Improved computational efficiency by developing an approximate analytical solution of PDEs for Li-ion diffusion.
3. Integrated the enhanced battery electro-chemical model into the framework for multi-objective optimization of S-HEV supervisory control. This increased the number of states to five, and made the solution intractable using the SDP algorithm. Therefore, developed a new framework based on Neuro Dynamic Programming (NDP) algorithm, and demonstrated its ability to handle the larger state-action space. Solution demonstrated further benefits in simultaneous optimization of fuel efficiency and battery life.

In summary, this dissertation advances the knowledge in the field of optimal supervisory control design for series HEV systems. Auxiliary cooling consumption was considered in addition to vehicle propulsion, and battery thermal management and power management was integrated in the optimization of supervisory control. Battery side reaction associated with SEI growth was considered into system-level study; the thermal effect and lithium ions diffusion delay was considered in the modeling of reaction rate. NDP algorithm's to handle the extended system model with large state-action space has been demonstrated, and results quantify the potential for extending battery life while preserving the fuel efficiency potential of S-HEV.

6.3 Perspectives on Future Work

There exists several opportunities to advance the work presented here, in both system modeling and optimization algorithm.

First, the system model could extend to considering engine thermal management. To reduce battery cooling loss, battery load cycle becomes milder. However, this results in the increase of engine heat generation. Engine cooling loss should be considered. Second, the fidelity of battery aging model can be enhanced by further considering the diffusion delay in electrolyte. This is mainly important under high C-rate charging or discharging. Battery thermal model in optimization algorithm is simplified using the average temperature. The resulting control strategy can cause highly uneven temperature distribution inside of battery cells. Reducing the temperature difference between battery core and surface could be considered as additional objective.

Opportunities also exist for improvement in neuro dynamic programming. The algorithm runs with system model. The policy used is greedy policy based on approximated value function, and a numerical optimization process based on system model is required to compute the policy. An alternative method, policy search based on stochastic gradient method, can be adopted to replace greedy policy for online model-free control, which could be adaptive.

REFERENCES

G. Khalil, "Challenges of hybrid electric vehicles for military applications," 2009 IEEE Vehicle Power and Propulsion Conference, Dearborn, MI, 2009, pp. 1-3. doi: 10.1109/VPPC.2009.5289878

R. Van Haaren, "Assessment of electric cars' range requirements and usage patterns based on driving behavior recorded in the National Household Travel Survey of 2009, " Earth and Environment Engineering Department, Columbia University, Fu Foundation School of Engineering and Applied Science, New York, NY (2011)

Smith, K.W., Eric; Santhanagopalan, Shriram; Kim, Gi-Heon; Shi, Ying; Pesaran, Ahmad, "Predictive Models of Li-ion Battery Lifetime", in Advanced Automotive & Industrial/Stationary Battery Conference. 2015: Detroit, Michigan. P. 24.

E.V. Thomas, I. Bloom, J.P. Christophersen, V.S. Battaglia, Statistical methodology for predicting the life of lithium-ion cells via accelerated degradation testing, Journal of Power Sources, Volume 184, Issue 1, 15 September 2008, Pages 312-317, ISSN 0378-7753

Kim, Y. J. and Filipi, Z., "Series hydraulic hybrid propulsion for a light truck-optimizing the thermostatic power management". SAE Technical Paper (No. 2007-24-0080)

N. Jalil, N. A. Kheir and M. Salman, "A rule-based energy management strategy for a series hybrid vehicle," American Control Conference, 1997. Proceedings of the 1997, Albuquerque, NM, 1997, pp. 689-693 vol.1., doi: 10.1109/ACC.1997.611889.

M. Salman, N. J. Schouten and N. A. Kheir, "Control strategies for parallel hybrid vehicles," American Control Conference, 2000. Proceedings of the 2000, Chicago, IL, 2000, pp. 524-528 vol.1, doi: 10.1109/ACC.2000.878955

T. Hofman, R.M. van Druten, M. Steinbuch, A.F.A. Serrarens, Rule-Based Equivalent Fuel Consumption Minimization Strategies for Hybrid Vehicles, IFAC Proceedings Volumes, Volume 41, Issue 2, 2008, Pages 5652-5657, ISSN 1474-6670

Johri, R. and Filipi, Z., "Low-Cost Pathway to Ultra Efficient City Car: Series Hydraulic Hybrid System with Optimized Supervisory Control," SAE Int. J. Engines 2(2):505-520, 2010, doi:10.4271/2009-24-0065.

Serrao, L., Onori, S., Rizzoni, G., "A comparative analysis of energy management strategies for hybrid electric vehicles", ASME Journal of Dynamic Systems, Measurement and Control, Vol. 133, pp. 1–9, 2011

Serrao, L., Onori, S., Rizzoni, G., "Equivalent Consumption Minimization Strategy as a realization of Pontryagin¹s minimum principle for HEV control", 2009 American Control Conference, St. Louis, Missouri, USA June 10 - 12, 2009

Gu B., Rizzoni G. (2006) An adaptive algorithm for hybrid electric vehicle energy management based on driving pattern recognition, Proceedings of the ASME 2006 International Mechanical Engineering Congress and Exposition (IMEC 2006), Chicago, IL, USA, 5-10 Nov

Onori, S., Serrao, L., Rizzoni, G., "Adaptive equivalent consumption minimization strategy for HEVs", 2010 ASME Dynamic Systems and Control Conference, Cambridge, MA, Sept. 13-15

J. Lescot, A. Sciarretta, Y. Chamaillard and A. Charlet, "On the integration of optimal energy management and thermal management of hybrid electric vehicles," 2010 IEEE Vehicle Power and Propulsion Conference, Lille, 2010, pp. 1-6. doi: 10.1109/VPPC.2010.5729158

A. Chasse, G. Corde, A. Del Mastro and F. Perez, "Online optimal control of a parallel hybrid with after-treatment constraint integration," 2010 IEEE Vehicle Power and Propulsion Conference, Lille, 2010, pp. 1-6. doi: 10.1109/VPPC.2010.5729166

N. Kim, S. Cha and H. Peng, "Optimal Control of Hybrid Electric Vehicles Based on Pontryagin's Minimum Principle," in IEEE Transactions on Control Systems Technology, vol. 19, no. 5, pp. 1279-1287, Sept. 2011. doi: 10.1109/TCST.2010.2061232

Kim, N. and A. Rousseau, "Sufficient conditions of optimal control based on Pontryagin's minimum principle for use in hybrid electric vehicles," Proceedings of the Institution of Mechanical Engineers, Part D: Journal of Automobile Engineering, 2012. 226(9): p. 1160-1170.

L. Tang, G. Rizzoni and S. Onori, "Optimal energy management of HEVs with consideration of battery aging," Transportation Electrification Asia-Pacific (ITEC Asia-Pacific), 2014 IEEE Conference and Expo, Beijing, 2014, pp. 1-6. doi: 10.1109/ITEC-AP.2014.6941202

Nüesch, Tobias; Cerofolini, Alberto; Mancini, Giorgio; Cavina, Nicolò; Onder, Christopher; Guzzella, Lino. 2014. "Equivalent Consumption Minimization Strategy for the Control of Real Driving NOx Emissions of a Diesel Hybrid Electric Vehicle." Energies 7, no. 5: 3148-3178.

G. Rousseau, D. Sinoquet, and P. Rouchon, "Constrained Optimization of Energy Management for a Mild-Hybrid Vehicle," Oil & Gas Science and Technology - Revue de l'IFP, 2007. 62(4): p. 623-634. doi: 10.2516/ogst:2007056

D. Maamria, F. Chaplais, N. Petit and A. Sciarretta, "Comparison of several strategies for HEV energy management system including engine and catalyst temperatures," 2015 American Control Conference (ACC), Chicago, IL, 2015, pp. 2948-2955. doi: 10.1109/ACC.2015.7171183

H. A. Borhan, A. Vahidi, A. M. Phillips, M. L. Kuang, and I. V. Kolmanovsky, "Predictive energy management of a power-split hybrid electric vehicle," 2009 American Control Conference, St. Louis, MO, 2009, pp. 3970-3976. doi: 10.1109/ACC.2009.5160451

H. Borhan, A. Vahidi, A. M. Phillips, M. L. Kuang, I. V. Kolmanovsky and S. Di Cairano, "MPC-Based Energy Management of a Power-Split Hybrid Electric Vehicle," in IEEE Transactions on Control Systems Technology, vol. 20, no. 3, pp. 593-603, May 2012. doi: 10.1109/TCST.2011.2134852

V. T. Minh and A. A. Rashid, "Modeling and model predictive control for hybrid electric vehicles," International Journal of Automotive Technology, 2012, 13(3): p. 477-485.

Wu B, Lin CC, Filipi Z, Peng H, Assanis D. Optimal power management for a hydraulic hybrid delivery truck. Vehicle System Dynamics. 2004 Jul;42(1-2):23-40. Available from, DOI: 10.1080/00423110412331291562.

Neuman, M., Sandberg, H. And Wahlberg, B., "Rule-Based Control of Series HEVs Derived from Deterministic Dynamic Programming", Submitted to American Control Conference 2009.

Lin, X., Ivanco, A., and Filipi, Z., "Optimization of Rule-Based Control Strategy for a Hydraulic-Electric Hybrid Light Urban Vehicle Based on Dynamic Programming," SAE Int. J. Alt. Power. 1(1):249-259, 2012, doi:10.4271/2012-01-1015.

S. Ebbesen, P. Elbert and L. Guzzella, "Battery State-of-Health Perceptive Energy Management for Hybrid Electric Vehicles," in IEEE Transactions on Vehicular Technology, vol. 61, no. 7, pp. 2893-2900, Sept. 2012. doi: 10.1109/TVT.2012.2203836

Lin, X, Perez, HE, Siegel, JB, Stefanopoulou, AG, Li, Y, Anderson, RD, Ding, Y & Castanier, MP 2013, 'Online parameterization of lumped thermal dynamics in cylindrical lithium ion batteries for core temperature estimation and health monitoring' IEEE Transactions on Control Systems Technology, vol 21, no. 5, 6320619, pp. 1745-1755. DOI: 10.1109/TCST.2012.2217143

Ebbesen, Soren, and Lino Guzzella. "Trade-off between fuel economy and battery life for hybrid electric vehicles." In ASME 2011 Dynamic Systems and Control Conference and Bath/ASME Symposium on Fluid Power and Motion Control, pp. 217-223. American Society of Mechanical Engineers, 2011.

L. Johannesson, M. Asbogard and B. Egardt, "Assessing the Potential of Predictive Control for Hybrid Vehicle Powertrains Using Stochastic Dynamic Programming," in IEEE Transactions on Intelligent Transportation Systems, vol. 8, no. 1, pp. 71-83, March 2007. doi: 10.1109/TITS.2006.884887

Moura, S.J., J.L. Stein, and H.K. Fathy, Battery-Health Conscious Power Management in Plug-In Hybrid Electric Vehicles via Electrochemical Modeling and Stochastic Control. Control Systems Technology, IEEE Transactions on, 2013. 21(3): p. 679-694.

Xiaosong Hu, Shengbo Li, Huei Peng, A comparative study of equivalent circuit models for Li-ion batteries, Journal of Power Sources, Volume 198, 15 January 2012, Pages 359-367, ISSN 0378-7753.

Johri, R., Filipi, Z., “Optimal Energy Management of a Series Hybrid Vehicle with Combined Fuel Economy and Low Emission Objectives”, Proc. IMechE, Part D: Journal of Automobile Engineering, October 2014, vol. 228 no. 12, pp. 1424-1439

Johri, R., Filipi, Z.,” Neuro-Fuzzy Model Tree Approach to Virtual Sensing of Transient Diesel Soot and NOx Emissions", International Journal of Engine Research, December 2014 vol. 15 no. 8, pp. 918-927

Johri, R., Filipi, Z., “Low-Cost Pathway to Ultra Efficient City Car: Series Hydraulic Hybrid System with Optimized Supervisory Control”, SAE Paper 2009-24-0065, SAE Journal of Engines, also presented at the ICE2009 Conference, Capri, Italy, September 2009

Johri, R., Salvi, A., and Filipi, Z., “Optimal Energy Management for a Hybrid Vehicle Using Neuro-Dynamic Programming to Consider Transient Engine Operation,” Proceedings of the 4th Annual ASME Dynamic Systems and Control Conference, Arlington, VA, 2011

Johri, R., Filipi, Z., “Self-Learning Neural Controller for Hybrid Power Management using Neuro-Dynamic Programming“, SAE paper 2011-24-0081, 10th International ICE2011 Conference, Capri, Italy, September 2011

J. Vetter, P. Novák, M.R. Wagner, C. Veit, K.-C. Möller, J.O. Besenhard, M. Winter, M. Wohlfahrt-Mehrens, C. Vogler, A. Hammouche, Ageing mechanisms in lithium-ion batteries, Journal of Power Sources, Volume 147, Issues 1–2, 9 September 2005, Pages 269-281, ISSN 0378-7753

Dirk Uwe Sauer, Heinz Wenzl, Comparison of different approaches for lifetime prediction of electrochemical systems—Using lead-acid batteries as example, Journal of Power Sources, Volume 176, Issue 2, 1 February 2008, Pages 534-546, ISSN 0378-7753

John Wang, Ping Liu, Jocelyn Hicks-Garner, Elena Sherman, Souren Soukiazian, Mark Verbrugge, Harshad Tataria, James Musser, Peter Finamore, Cycle-life model for graphite-LiFePO4 cells, Journal of Power Sources, Volume 196, Issue 8, 15 April 2011, Pages 3942-3948, ISSN 0378-7753.

Fabio Todeschini, Simona Onori, Giorgio Rizzoni, An experimentally validated capacity degradation model for Li-ion batteries in PHEVs applications, IFAC Proceedings Volumes, Volume 45, Issue 20, January 2012, Pages 456-461, ISSN 1474-6670

Onori, S, Spagnol, P, Marano, V, Guezennec, Y & Rizzoni, G 2012, 'A new life estimation method for lithium-ion batteries in plug-in hybrid electric vehicles applications' International Journal of Power Electronics, vol 4, no. 3, pp. 302-319. DOI: 10.1504/IJPELEC.2012.046609

Andrea Cordoba-Arenas, Simona Onori, Yann Guezennec, Giorgio Rizzoni, Capacity and power fade cycle-life model for plug-in hybrid electric vehicle lithium-ion battery cells containing blended spinel and layered-oxide positive electrodes, Journal of Power Sources, Volume 278, 15 March 2015, Pages 473-483, ISSN 0378-7753

Suri, G & Onori, S 2016, 'A control-oriented cycle-life model for hybrid electric vehicle lithium-ion batteries' Energy, vol 96, pp. 644-653. DOI: 10.1016/j.energy.2015.11.075

Newman, J. and K.E. Thomas-Alyea, Electrochemical Systems, 2004, John Wiley & Sons

M. Safari, M. Morcrette, A. Teyssot, and C. Delacourt, Multimodal Physics-Based Aging Model for Life Prediction of Li-Ion Batteries, J. Electrochem. Soc. 2009 156(3): A145-A153; doi:10.1149/1.3043429

Guo, M., G. Sikha, and R.E. White, Single-Particle Model for a Lithium-Ion Cell: Thermal Behavior, Journal of the Electrochemical Society, 2011. 158(2): p. A122.

Ning, G. and B.N. Popov, Cycle Life Modeling of Lithium-Ion Batteries, Journal of the Electrochemical Society, 2004. 151(10): p. A1584.

P. Ramadass, Bala Haran, Parthasarathy M. Gomadam, Ralph White, and Branko N. Popov, Development of First Principles Capacity Fade Model for Li-Ion Cells, J. Electrochem. Soc. 2004 151(2): A196-A203; doi:10.1149/1.1634273

Long Cai, Yiling Dai, Marjorie Nicholson, Ralph E. White, Kamakshi Jagannathan, Garima Bhatia, Life modeling of a lithium ion cell with a spinel-based cathode, Journal of Power Sources, Volume 221, 1 January 2013, Pages 191-200, ISSN 0378-7753

Xianke Lin, Jonghyun Park, Lin Liu, Yoonkoo Lee, A. M. Sastry, and Wei Lu, A Comprehensive Capacity Fade Model and Analysis for Li-Ion Batteries, J. Electrochem. Soc. 2013 160(10): A1701-A1710; doi:10.1149/2.040310jes

Darling, R. and J. Newman, Modeling Side Reactions in Composite Li y Mn2 O 4 Electrodes, Journal of the Electrochemical Society, 1998, 145(3): p. 990-998.

Christensen, J. and J. Newman, Effect of Anode Film Resistance on the Charge/Discharge Capacity of a Lithium-Ion Battery, Journal of the Electrochemical Society, 2003. 150(11): p. A1416.

Ploehn, H.J., P. Ramadass, and R.E. White, Solvent Diffusion Model for Aging of Lithium-Ion Battery Cells, Journal of the Electrochemical Society, 2004. 151(3): p. A456.

E. Prada, D. Di Domenico, Y. Creff, J. Bernard, V. Sauvant-Moynot, and F. Huet, A Simplified Electrochemical and Thermal Aging Model of LiFePO4-Graphite Li-ion Batteries: Power and Capacity Fade Simulations, J. Electrochem. Soc. 2013 160(4): A616-A628; doi:10.1149/2.053304jes

Venkatasailanathan Ramadesigan, Paul W. C. Northrop, Sumitava De, Shriram Santhanagopalan, Richard D. Braatz, and Venkat R. Subramanian, Modeling and Simulation of Lithium-Ion Batteries from a Systems Engineering Perspective, J. Electrochem. Soc. 2012 159(3): R31-R45; doi:10.1149/2.018203jes

X. Hu, H. Perez, and S. J. Moura, “Battery charge control with an electro-thermal-aging coupling,” in 2015 ASME Dynamic Systems and Control Conference, Columbus, OH, 2015.

Scott J. Moura, M.K.a.N.A.C. Adaptive PDE Observer for Battery SOC/SOH Estimation, in ASME 2012 5th Annual Dynamic Systems and Control Conference 2012. Fort Lauderdale, Florida, USA.

Dey, S., B. Ayalew, and P. Pisu, Combined estimation of State-of-Charge and State-of-Health of Li-ion battery cells using SMO on electrochemical model. in 2014 13th International Workshop on Variable Structure Systems (VSS). 2014.

A. Sciarretta, D. di Domenico, P. Pognant-Gros, and G. Zito, Optimal Energy Management of Automotive Battery Systems Including Thermal Dynamics and Ageing, to appear in Optimization and Optimal Control in Automotive Systems, Springer Lecture Notes in Control Science, 2014. 455: p. 219-236.

Serrao, L., et al. Optimal energy management of hybrid electric vehicles including battery aging. in American Control Conference (ACC), 2011. 2011.

Rahn, C.D. and C.-Y. Wang, Discretization Methods, in Battery Systems Engineering. 2013, John Wiley & Sons Ltd. p. 49-87.

Meng Guo, Ralph E. White, An approximate solution for solid-phase diffusion in a spherical particle in physics-based Li-ion cell models, Journal of Power Sources, Volume 198, 15 January 2012, Pages 322-328, ISSN 0378-7753

Beers, K.J., Numerical Methods for Chemical Engineering: Applications in MATLAB. 2007: Cambridge University Press.

Christophe Forgez, Dinh Vinh Do, Guy Friedrich, Mathieu Morcrette, Charles Delacourt, Thermal modeling of a cylindrical LiFePO4/graphite lithium-ion battery, Journal of Power Sources, Volume 195, Issue 9, 1 May 2010, Pages 2961-2968, ISSN 0378-7753.

Moran, M.J., Shapiro, H.N., Boettner, D.D., and Bailey, M.B., Fundamentals of Engineering Thermodynamics, John Wiley & Sons, 2010

Tao, X. and Wagner, J. R. (2014). Cooling air temperature and mass flow rate control for hybrid electric vehicle battery thermal management. In ASME 2014 DynamicSystems and Control Conference, pages V002T34A002–V002T34A002. American Society of Mechanical Engineers.

Chan-Chiao Lin, Huei Peng, J. W. Grizzle and Jun-Mo Kang, "Power management strategy for a parallel hybrid electric truck," in IEEE Transactions on Control Systems Technology, vol. 11, no. 6, pp. 839-849, Nov. 2003. doi: 10.1109/TCST.2003.815606

Chan-Chiao Lin, Huei Peng and J. W. Grizzle, "A stochastic control strategy for hybrid electric vehicles," American Control Conference, 2004. Proceedings of the 2004, Boston, MA, USA, 2004, pp. 4710-4715 vol.5.

S. J. Moura, H. K. Fathy, D. S. Callaway and J. L. Stein, "A Stochastic Optimal Control Approach for Power Management in Plug-In Hybrid Electric Vehicles," in IEEE Transactions on Control Systems Technology, vol. 19, no. 3, pp. 545-555, May 2011. doi: 10.1109/TCST.2010.2043736

Sutton, Richard S., and Andrew G. Barto. Reinforcement learning: An introduction. Vol. 1, no. 1. Cambridge: MIT press, 1998.

Powell, Warren B. Approximate Dynamic Programming: Solving the curses of dimensionality. Vol. 703. John Wiley & Sons, 2007.